An Overlay J_2 Viscoelastic Viscoplastic Viscodamage Model for Stable Shear Localization Problems

M. Cervera
M. Chiumenti

Monograph CIMNE Nº-85, September 2003

An Overlay J_2 Viscoelastic Viscoplastic Viscodamage Model for Stable Shear Localization Problems

M. Cervera
M. Chiumenti
International Center for Numerical Methods in Engineering (CIMNE)
Technical University of Catalonia (UPC)

Monograph CIMNE Nº-85, September 2003

INTERNATIONAL CENTER FOR NUMERICAL METHODS IN ENGINEERING
Gran Capitán s/n, 08034 Barcelona, Spain

INTERNACIONAL CENTER FOR NUMERICAL METHODS IN ENGINEERING
Edificio C1, Campus Norte UPC
Gran Capitán s/n
08034 Barcelona, Spain
www.cimne.upc.es

First edition: September 2003

AN OVERLAY J_2 VISCOELASTIC VISCOPLASTIC VISCODAMAGE MODEL FOR STABLE SHEAR LOCALIZATION PROBLEMS

Monograph CIMNE M85

ISBN: 84-95999-41-2

Depósito legal: B-40328-2003

Abstract

This work formulates a relatively simple isotropic local *Overlay* J_2-*Viscoelastic*-*Viscoplastic*-*Viscodamage* constitutive model (O-J_2-VVV) which encompasses the merits of both the plastic and continuum damage formulations. The plastic component of the model account for inelastic permanent strains, while the damage component account for loss of stiffness. The plastic and damage softening moduli are regularized according to the material mode II fracture energy and the element size. The *Orthogonal SubGrid Stabilization* Method ($OSGS$) is used to ensure existance and uniquess of the solution for strain shear strain localization processes, attaining global and local stability of the corresponding discrete finite element formulation. Consistent residual viscosity is used to enhance robustness and convergence of the formulation. Numerical examples show that the formulation derived is versatily, fully stable and remarkably robust, The solutions obtained are completely mesh independent, unlike those obtained with the ill-posed standard approaches.

1 Introduction

Softening materials subjected to monotonic straining exhibit *strain localization*. In particular, in the so-called J_2 materials, shear (or slip) strains concentrate, under certain circumstances. This phenomenon leads to the formation of *shear bands* inside the solid where, once the peak stress is reached, the deformation concentrates while the material outside the band unloads. Shear bands are typical of ductile materials such as metals, although they are also observed in granular materials such as sands or soils. Similar deformation patterns can also appear in fiber-reinforced composites subjected to compressive loading.

Upon continuing straining, the width of the shear band diminishes and, unless there is a physical limitation, it tends to zero. In J_2 materials, these zero width bands are called *slip lines*. It is generally accepted in fracture mechanics that the amount of energy released during the formation of a unit area of slip surface is a material property, called the *mode II fracture energy*.

Despite the considerable effort devoted to the subject in the last two decades, theoretical modeling and computational resolution of the strain localization process that gives place to shear bands and, ultimately, to structural failure due to them have remained an open challenge in Computational Solid Mechanics.

The possibilities to model shear bands with finite elements are several, and both the weak and the strong discontinuity approaches have been followed. In the first, the objective is to capture the shear band as precisely as possible, with standard continuous elements. In the second, the displacement field is enhanced with discontinuous functions so that the true slip line can be captured.

The main difficulty why most attempts to model weak displacement discontinuities with standard, local, approaches is that the solutions obtained appear to be unphysically, and unacceptably, fully determined by the fineness and ori-

entation of the discretization. Up to now, this disagreeable observation has been erroneously and misleadingly attributed to the fact that, when strain-softening occurs and the slope of the local stress-strain curve becomes negative, the governing equations of the Continuum Mechanics problem lose their "natural" elliptic character.

Recently, the authors have applied *stabilization methods* to the solution of J_2-plastic and J_2-damage problems with mixed displacement/pressure ($\mathbf{u}/p$) linear simplicial elements, see [1], [2], [3], [4] and [5]. This translates in the achievement of three important goals:

- (a) the solution of the corresponding localization boundary value problem exists and it is unique,
- (b) the position and orientation of the localization bands is independent of the directional bias of the finite element mesh, and
- (c) the global post-peak load-deflection curves are independent of the size of the elements in the localization band.

The accomplishment of these fundamental objectives is attained by ensuring both *global and local stability of the problem*; this is secured by the appropriate modification of the variational formulation, making use of the concept of *sub-grid* approximation.

In this work, we formulate an isotropic *Overlay J2-Viscoelastic-Viscoplastic-Viscodamage model (O-J_2-VVV model)* that encompasses the merits of both the plastic and continuum damage formulations. It must be emphasized that the choice of an isotropic model implies that the macroscopic anisotropy of the structural behaviour has to be captured by means of a finite element approximation to within the resolution of the adopted mesh [6], [7]. On the other hand, this provides a relatively simple constitutive model which, nevertheless, is very versatile and able to predict appropriately the softening response.

The outline of the monograph is as follows. In the first chapter, the mixed isotropic *O-J_2-VVV* model is presented. Constitutive relationships, evolution laws for the internal variables, consistent tangent operators and thermodynamic frameworks are proposed and discussed. The plastic and damage softening moduli are appropriately regularized according to the size of the elements inside the

localization band. In the second chapter, the corresponding mixed displacement/pressure ($\mathbf{u}/p$) boundary value problem is formulated and properly stabilized with the *Orthogonal SubGrid Scale (OSGS)* method. The possibility of enhancing the robustness and convergence of the numerical procedure by the inclusion of consistent residual plastic and damage viscosities is also considered. Finally, in the third chapter, numerical benchmarks and strain localization examples are presented to assess the present formulation.

2 Mixed formulation for J_2 models

2.1 Stress and strain tensors

The (second order) stress tensor $\boldsymbol{\sigma}$ can be expressed as:

$$\boldsymbol{\sigma} = p\mathbf{1} + \mathbf{s} \tag{2.1}$$

where $p = (1/3)\,\mathrm{tr}\,(\boldsymbol{\sigma})$ and $\mathbf{s} = \mathrm{dev}\,(\boldsymbol{\sigma})$ are the volumetric and the deviatoric parts of the stress tensor, respectively, and $\mathbf{1}$ is the (second order) unit tensor. Correspondingly, the (second order) strain tensor $\boldsymbol{\varepsilon} = \nabla^s \mathbf{u}$, where $\mathbf{u}$ are the displacements, is expressed as:

$$\boldsymbol{\varepsilon}(\mathbf{u}) = \frac{1}{3}\varepsilon_v \mathbf{1} + \mathbf{e} \tag{2.2}$$

where $\varepsilon_v = \mathrm{tr}\,\boldsymbol{\varepsilon} = \nabla \cdot \mathbf{u}$ and $\mathbf{e} = \mathrm{dev}\,\boldsymbol{\varepsilon}$ are the volumetric and the deviatoric parts of the strain tensor, respectively.

For linear elastic behaviour, the constitutive equations are simply expressed as:

$$p = K\varepsilon_v \tag{2.3a}$$
$$\mathbf{s} = 2G\,\mathrm{dev}\,\boldsymbol{\varepsilon} = 2G\mathbf{e} \tag{2.3b}$$

where K is the bulk modulus, also referred to as modulus of volumetric compressibility, and G is the shear modulus.

2.2 J_2 Viscoelasticity

2.2.1 Constitutive model

In classical viscoelasticity, the mechanical behaviour is characterized by the relaxation function or the compliance function and the constitutive relationships are formulated in the form of Volterra integral equations [8]. This approach is clearly unsuitable for numerical computations because of its memory and CPU time requirements.

However, it is possible to expand any relaxation function into a Dirichlet series, and retain only a finite number of terms. This achieves a double goal: first, the constitutive laws for the viscoelastic material can be written in terms of a finite number of internal variables, and only these need to be stored from one time step to the next, thus providing huge computational advantages compared to the hereditary integral equations; and secondly, the resulting rheological model can be interpreted as a generalized Maxwell chain, where a number of springs and dashpots are arranged in parallel. Alternatively, the compliance function of concrete can be considered and expanded in a Dirichlet series. This leads to a generalized Kelvin chain with a series arrangement. Although both approaches are completely equivalent (if a large enough number of terms is considered in the Maxwell or Dirichlet series), the first one leads to first order differential equations to be solved for the evolution of the internal variables, while the second approach leads to second order differential equations [9]. Therefore, the Maxwell chain model is preferred here.

In the following, we will consider that the Eq. (2.3a) holds, while the deviatoric stresses are obtained from the J_2-viscoelastic model proposed below.

Figure 2.1 shows a schematic representation of the rheological model used, in the form of a Maxwell chain. The shear moduli, G^i, and the dashpot viscosities, η^i, of the $i = 0, 1, ..., N$ Maxwell elements of the chain are the material parameters. Alternatively, the chain may be characterized by the elastic shear moduli, G^i, and the relaxation times of the dashpots, defined as $\vartheta^i = \eta^i / G^i$.

It is often convenient to take $\vartheta^0 = \infty$ in the series expansion, so that G^0 can be considered as the *asymptotic* (for time $t \to \infty$) material shear modulus. Note that $G = \sum_{i=0}^{N} G^i$ is the *instantaneous* (for time $t \to 0^+$) material shear modulus of.

It is also useful to define the *participation ratio* for each element in the chain,

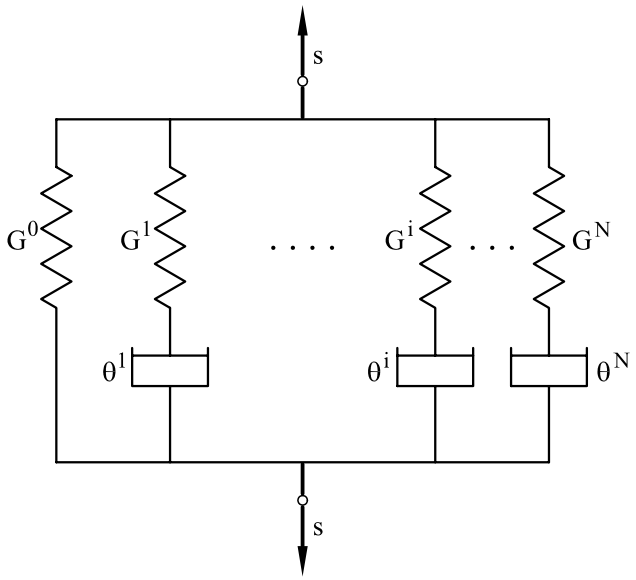

Fig. 2.1: Viscoelastic Maxwell chain

ξ^i,as the ratio between its own elastic modulus and that of the chain: $\xi^i = G^i/G$. Note that $\sum_{i=0}^{N} \xi^i = 1$.

The total deviatoric stress sustained by the (parallel) Maxwell chain is evaluated as

$$\mathbf{s} = \sum_{i=0}^{N} \mathbf{s}^i \tag{2.4}$$

Choosing the stress in each Maxwell element of the chain, $\mathbf{s}^i$, as internal variables, the first order differential equations governing the evolution of these variables are

$$\dot{\mathbf{s}}^i + \frac{\mathbf{s}^i}{\vartheta^i} = \xi^i \; 2G \, \dot{\mathbf{e}} \quad \text{for} \quad i = 0, 1, ..., N \tag{2.5}$$

where $\mathbf{e}$ is the total deviatoric strain tensor. It is possible to select the viscous deviatoric strains in each Maxwell element, $\mathbf{e}^i$, rather than the deviatoric stress, $\mathbf{s}^i$, as internal variables. The relationship between them is

$$\mathbf{s}^i = \xi^i \; 2G \, (\mathbf{e} - \mathbf{e}^i) \tag{2.6}$$

Substitution of Eq. (2.6) into Eq. (2.5) leads to the obtention of the evolution

law for the viscous deviatoric strains

$$\dot{\mathbf{e}}^i = \frac{1}{\vartheta^i}\left(\mathbf{e} - \mathbf{e}^i\right) \qquad \text{for} \quad i = 0, 1, ..., N \tag{2.7}$$

2.2.2 Integration of the internal variables

The solution in time of the evolution law for the viscous deviatoric strains, Eq. (2.7) , is [10]:

$$\mathbf{e}^i = \frac{1}{\vartheta^i}\int_{-\infty}^{t} e^{-\frac{t-s}{\vartheta^i}}\mathbf{e}(s)\,ds \tag{2.8}$$

This can be expressed, for time $t_{n+1} = t_n + \Delta t$ as

$$\begin{aligned}
\mathbf{e}^i(t_{n+1}) &= \frac{1}{\vartheta^i}\int_{-\infty}^{t_{n+1}} e^{-\frac{(t_{n+1})-s}{\vartheta^i}}\mathbf{e}(s)\,ds \\
&= \frac{1}{\vartheta^i}\int_{-\infty}^{t_n} e^{-\frac{(t_n-s)}{\vartheta^i}} e^{-\frac{\Delta t}{\vartheta^i}}\mathbf{e}(s)\,ds + \\
&\qquad + \frac{1}{\vartheta^i}\int_{-\infty}^{t_{n+1}} e^{-\frac{(t_{n+1})-s}{\vartheta^i}}\mathbf{e}(s)\,ds \\
&= \mathbf{e}^i(t_n)\, e^{-\frac{\Delta t}{\vartheta^i}} + \Delta\mathbf{e}^i
\end{aligned} \tag{2.9}$$

with the increment of viscous deviatoric strain equal to the second integral term

$$\Delta\mathbf{e}^i = \frac{1}{\vartheta^i}\int_{-\infty}^{t_{n+1}} e^{-\frac{(t_{n+1})-s}{\vartheta^i}}\mathbf{e}(s)\,ds \tag{2.10}$$

The numerical integration of Eq. (2.10) can be performed by different methods. Here, we will assume that the deviatoric strain is approximately constant during the interval $[t_n, t_{n+1}]$ and equal to the value at time t^*, (with $t^* = t_n + \alpha\Delta t$, $0 \le \alpha \le 1$). Then, Eq. (2.10) can be evaluated as

$$\begin{aligned}
\Delta\mathbf{e}^i &= \frac{1}{\vartheta^i}\mathbf{e}(t^*)\int_{-\infty}^{t_{n+1}} e^{-\frac{t_{n+1}}{\vartheta^i}} e^{\frac{s}{\vartheta^i}}\,ds \\
&= \mathbf{e}(t^*)\, e^{-\frac{t_{n+1}}{\vartheta^i}}\left[e^{\frac{s}{\vartheta^i}}\right]_{t_n}^{t_{n+1}} \\
&= \mathbf{e}(t^*)\left(1 - e^{-\frac{\Delta t}{\vartheta^i}}\right)
\end{aligned} \tag{2.11}$$

and, therefore, Eq. (2.9) is

$$\boldsymbol{\varepsilon}^i(t_{n+1}) = \boldsymbol{\varepsilon}^i(t_n)\, e^{-\frac{\Delta t}{\vartheta^i}} + \boldsymbol{\varepsilon}(t^*)\left(1 - e^{-\frac{\Delta t}{\vartheta^i}}\right) \tag{2.12}$$

Taking $\alpha = 0$, $t^* = t_n$ and it is necessary to store $\boldsymbol{\varepsilon}(t_n)$ to integrate the viscous strains. It is, therefore, computationally more efficient to use $\alpha = 1$, $t^* = t_{n+1}$, and then Eq. (2.9) reduces to

$$\mathbf{e}^i(t_{n+1}) = \mathbf{e}^i(t_n)\, e^{-\frac{\Delta t}{\vartheta^i}} + \mathbf{e}(t_{n+1}) \left(1 - e^{-\frac{\Delta t}{\vartheta^i}}\right) \tag{2.13}$$

It must be remarked that this integration method is *unconditionally stable*.

For small time steps, $\Delta t/\vartheta^i << 1$, $e^{-\frac{\Delta t}{\vartheta^i}} \simeq 1 - (\Delta t/\vartheta^i)$, and Eq. (2.13) can be rewritten as

$$\mathbf{e}^i(t_{n+1}) = \mathbf{e}^i(t_n) \; + \frac{\Delta t}{\vartheta^i} \left[\mathbf{e}(t_{n+1}) - \mathbf{e}^i(t_n)\right] \tag{2.14}$$

which obviously corresponds to a backward Euler scheme.

2.2.3 Tangent operator

The tangent operator consistent with the numerical integration scheme proposed can be obtained by differentiating Eq. (2.4) with respect to time, substituting Eq. (2.6), and differentiating the integration scheme Eq. (2.13), to obtain:

$$\begin{aligned}
\dot{\mathbf{s}} &= \sum_{i=0}^{N} \dot{\mathbf{s}}^i \\
&= \sum_{i=0}^{N} \xi^i 2G(\dot{\mathbf{e}} - \dot{\mathbf{e}}^i) \\
&= \left[\sum_{i=0}^{N} \xi^i e^{-\frac{\Delta t}{\vartheta^i}}\right] \mathbf{C}_{\text{dev}} : \dot{\boldsymbol{\varepsilon}} \\
&= \mathbf{C}_{\text{dev}}^{\text{visc}} : \dot{\boldsymbol{\varepsilon}}
\end{aligned} \tag{2.15}$$

where $\mathbf{C}_{\text{dev}} = 2G\left[\mathbf{I} - \frac{1}{3}(\mathbf{1} \otimes \mathbf{1})\right]$ is the standard (fourth order) linear–elastic deviatoric constitutive tensor, $\mathbf{I}$ is the (fourth order) unit tensor and (:) denotes the tensor product contracted on two indices. Note that, in this model, $\dot{\boldsymbol{\varepsilon}}^i = \dot{\mathbf{e}}^i$.

Therefore, the viscoelastic deviatoric tangent operator is

$$\mathbf{C}_{\text{dev}}^{\text{visc}} = \left[\sum_{i=0}^{N} \xi^i e^{-\frac{\Delta t}{\vartheta^i}}\right] \mathbf{C}_{\text{dev}} \tag{2.16}$$

Note that for very small time steps, $\Delta t/\vartheta^i \to 0$, the viscoelastic operator is purely elastic, $\mathbf{C}_{\rm dev}^{\rm visc} \to \mathbf{C}_{\rm dev}$. Also, for large time steps, $\Delta t/\vartheta^i >> 1$, the response tends to be asymptotic, $\mathbf{C}_{\rm dev}^{\rm visc} \to (G^0/G)\ \mathbf{C}_{\rm dev}$.

2.2.4 Thermodynamic Framework

Let us define the mechanical free energy for the viscoelastic model in the form

$$
\begin{aligned}
W^e &= W_{\rm vol}\,(\varepsilon_v) + W_{\rm dev}(\mathbf{e}, \mathbf{e}_e^i) && \text{(2.17a)}\\
&= \frac{1}{2}\,K\,\varepsilon_v^2 + \sum_{i=0}^{N} W_{\rm dev}^i(\mathbf{e}_e^i) && \text{(2.17b)}\\
&= \frac{1}{2}\,K\,\varepsilon_v^2 + \sum_{i=0}^{N} \frac{1}{2}\,\mathbf{e}_e^i : (\xi^i\ \mathbf{C}_{\rm dev}) : \mathbf{e}_e^i && \text{(2.17c)}
\end{aligned}
$$

where the elastic deviatoric strain tensor is defined as $\mathbf{e}_e^i = \mathbf{e} - \mathbf{e}^i$, for each element.

Using Coleman's method, the total stress can be obtained as

$$
\begin{aligned}
p &= \partial_{\varepsilon_v}\ K\varepsilon_v && \text{(2.18a)}\\
\mathbf{s} &= \sum_{i=0}^{N} \partial_{\mathbf{e}_e^i} W_{\rm dev}^i \;=\; \sum_{i=0}^{N} \xi^i\,\mathbf{C}_{\rm dev} : \mathbf{e}_e^i \;=\; \sum_{i=0}^{N} \mathbf{s}^i && \text{(2.18b)}
\end{aligned}
$$

Note that the introduced viscous deviatoric strains $\mathbf{e}^i$ are the thermodynamic forces conjugated to the deviatoric stresses in the chain elements $\mathbf{s}^i$ ($\mathbf{s}^i = -\partial_{\mathbf{e}^i} W_{\rm dev}$). Also, the mechanical dissipation for the Maxwell chain can be computed as

$$
\dot{\mathcal{D}} = \sum_{i=0}^{N} \frac{2}{\vartheta^i}\, W_{\rm dev}^i \;\geq\; 0 \qquad \text{(2.19)}
$$

2.3 J_2 Viscoplasticity

2.3.1 Constitutive equation

The constitutive equations for a J_2-viscoplastic model are :

$$
\begin{aligned}
p &= K\varepsilon_v && \text{(2.20a)}\\
\mathbf{s} &= 2G\mathbf{e}^e && \text{(2.20b)}
\end{aligned}
$$

where ε_v is the total volumetric strain and $\mathbf{e}^e$ is the *elastic* deviatoric strain tensor, defined as:

$$\mathbf{e}^e = \mathbf{e} - \mathbf{e}^p \tag{2.21}$$

where $\mathbf{e}^p$ is the plastic strain tensor, which in J_2 plasticity is purely deviatoric.

Let us define the *equivalent deviatoric plastic strain* in the usual manner, $\widetilde{e} = \left(\sqrt{2/3}\right) \int_o^t \|\dot{\mathbf{e}}^p\| \, dt$, and the *equivalent von Mises stress* as $\widetilde{s} = \left(\sqrt{3/2}\right) \|\mathbf{s}\| = \left(\sqrt{3/2}\right) \left[\, \mathbf{s} : \mathbf{s}\right]^{1/2}$. With these definitions, the rate of plastic work is $\dot{\mathcal{W}}^p = \mathbf{s} : \dot{\mathbf{e}}^p = \widetilde{s}\, \dot{\widetilde{e}}$.

2.3.2 Characterization of plastic behaviour

With the above definition for the equivalent effective stress, the plastic yield surface, Φ^p, is introduced as:

$$\Phi^p \left(\mathbf{s}, r^p\right) = \sqrt{\frac{3}{2}} \|\mathbf{s}\| - r^p = \widetilde{s} - r^p = 0 \tag{2.22}$$

Note that the plastic criterion is defined in the deviatoric stress space. In the principal stress space, the plastic criterion is the well-known von Mises cylinder with axis along the hydrostatic axis.

The isotropic softening variable $r^p = r^p(\widetilde{e})$ is an internal stress-like variable that defines the current size of the plastic yield surface, as it controls the value of the radius of the von Mises cylinder. In this work, we will consider both *linear* and *exponential* relationships between the equivalent deviatoric strain and the softening variable:

- *Linear softening:*

$$r^p = \begin{cases} \sigma_o \left(1 - \dfrac{H^p}{\sigma_o} \widetilde{e}\right) & 0 \leq \widetilde{e} \leq \dfrac{\sigma_o}{H^p} \\ 0 & \dfrac{\sigma_o}{H^p} \geq \widetilde{e} \end{cases} \tag{2.23}$$

- *Exponential softening:*

$$r^p = \sigma_o \exp\left(-\frac{2H^p}{\sigma_o} \widetilde{e}\right) \qquad 0 \leq \widetilde{e} \leq \infty \tag{2.24}$$

where $H^p \geq 0$ is a constant.

Notice that, in both cases, initially, when the equivalent deviatoric plastic strain $\widetilde{e} = 0, r^p$ is equal to the initial flow stress σ_o. Along the softening regime, r^p diminishes and, for large value of the equivalent plastic strain, it vanishes.

The evolution of the deviatoric plastic strain tensor is defined in the usual associative manner

$$\dot{\mathbf{e}}^p = \dot{\gamma}\,\mathbf{n} \tag{2.25}$$

where $\dot{\gamma}$ is the plastic multiplier and $\mathbf{n} = \partial\Phi^p/\partial\mathbf{s} = \mathbf{s}/\left\|\mathbf{s}\right\|$ is the normal to the yield surface.

For the rate independent case, the plastic multiplier $\dot{\gamma}$ is determined from the Kuhn-Tucker and consistency conditions:

$$\dot{\gamma} \;\geq\; 0 \qquad \Phi^p\left(\mathbf{s}, r^p\right) \leq 0 \qquad \dot{\gamma}\,\Phi^p\left(\mathbf{s}, r^p\right) = 0 \tag{2.26a}$$

$$\text{if } \Phi^p\left(\mathbf{s}, r^p\right) = 0 \;\text{ then }\; \dot{\gamma}\,\dot{\Phi}^p\left(\mathbf{s}, r^p\right) = 0 \tag{2.26b}$$

while for the rate dependent case, these conditions are replaced by a Perzyna-type relation:

$$\dot{\gamma} = \frac{\left\langle \Phi^p\left(\mathbf{s}, r^p\right)\right\rangle}{\eta^p} = \frac{\left\langle \Phi^p\left(\mathbf{s}, r^p\right)\right\rangle}{G\vartheta^p} \geq 0 \tag{2.27}$$

where $\langle\cdot\rangle$ are the Macaulay brackets (ramp function) and η^p is the plastic viscosity; $\vartheta^p := \eta^p/G$ is the retardation time for plastic behaviour. Notice that for very low values of the viscosity, $\eta^p \to 0$, or very small relaxation times, ϑ^p, the inviscid plastic model is recovered.

2.3.3 Coupling with viscoelasticy

The viscoplastic model described above can be easily coupled with the viscoelastic model described in Section 2.2. To this end, the definition of the deviatoric stresses, Eq. (2.20b), is simply replaced by its viscoelastic counterpart

$$\mathbf{s} = \sum_{i=0}^{N} \mathbf{s}^i \tag{2.28}$$

where $\mathbf{s}^i$ is the deviatoric stress sustained by each element of the Maxwell chain, computed as

$$\mathbf{s}^i \;=\; \xi^i\,\mathbf{C}_{\text{dev}} : \left(\mathbf{e} - \mathbf{e}^p - \mathbf{e}^i\right) \tag{2.29}$$

where ξ^i and $\mathbf{e}^i$ are the corresponding participation ratio and viscoelastic deviatoric strain tensor, respectively.

2.3.4 Integration of the internal variables

Details on the radial return algorithm to integrate along time both the elasto-plastic and the elasto-viscoplastic constitutive models can be found in reference [11].

2.3.5 Tangent Operator

The rate relationship between the deviatoric the strain and stress tensors can be written as

$$\dot{\mathbf{s}} = \left(\mathbf{C}_{\text{dev}}^{\text{tan}}\right)^p : \dot{\boldsymbol{\varepsilon}} \tag{2.30}$$

with

$$\begin{aligned}\left(\mathbf{C}_{\text{dev}}^{\text{tan}}\right)^p &= 2G \left\{ \left[\mathbf{I} - \frac{1}{3} (\mathbf{1} \otimes \mathbf{1}) \right] \left[\sum_{i=0}^{N} \xi^i e^{-\frac{\Delta t}{\vartheta^i}} \right] \right. \\ &\qquad \left. + \left[\delta_1 (\mathbf{1} \otimes \mathbf{1}) + \delta_2 (\mathbf{n} \otimes \mathbf{n}) \right] \right\}\end{aligned} \tag{2.31}$$

where the coefficients δ_1 and δ_2 depend on the radial return algorithm used (see reference [11] for details).

2.3.6 Thermodynamic Framework

Let us define the mechanical free energy for the (visco)elasto-viscoplastic model in the form

$$W = W_{\text{vol}}(\varepsilon_v) + W_{\text{dev}}(\mathbf{e}^e) \tag{2.32a}$$

$$= \frac{1}{2} K \varepsilon_v^2 + \frac{1}{2} (2G) (\mathbf{e} - \mathbf{e}^p) : (\mathbf{e} - \mathbf{e}^p) \tag{2.32b}$$

The constitutive equations for the model are obtained using Coleman's method as:

$$p = \partial_{\varepsilon_v} W = K \varepsilon_v \tag{2.33a}$$

$$\mathbf{s} = \partial_{\mathbf{e}} W = 2G \mathbf{e}^e \tag{2.33b}$$

The mechanical dissipation can be expressed as

$$\dot{\mathcal{D}} = \mathbf{s} : \dot{\mathbf{e}}^p = \mathbf{s} : \dot{\gamma}\mathbf{n} = \mathbf{s} : \dot{\gamma}\frac{\mathbf{s}}{\|\mathbf{s}\|} = \dot{\gamma} \quad \geq 0 \tag{2.34}$$

provided that the plastic multiplier increases monotonically, $\dot{\gamma} \geq 0$.

2.4 Softening behaviour and regularization

Either considering linear or exponential softening, the elasto-viscoplastic model described above is able to reproduce the softening branch that occurs in a test under monotonic shear straining after the peak stress is reached, with the stress decreasing asymptotically to the strain axis. With these evolution laws for r^p, a finite amount of energy is dissipated in the control volume.

In finite element analysis this entails the loss of objectivity of the results, in the sense that the inelastic shear strains tend to localize in a band that is only one element across, independently of the element size h_e. Upon mesh refinement, as h_e tends to zero, strains tend to concentrate on a band of zero thickness (a geometrical line), and no energy is dissipated in the failure process. Clearly, this is physically unacceptable.

In order to remedy this well-accounted for fact, reference [12] proposed the use of the so-called "*fracture energy regularization technique*", nowadays used in many FE applications. This strategy is followed in this work, as it is extremely convenient from the computational standpoint, while guaranteeing the correct conservation of dissipated energy upon mesh refinement.

It has to be remarked that this technique constitutes a crucial and appealing "lost-link" between Continuum and Fracture Mechanics, two disciplines that have often been presented as wide apart ways of approaching Failure Mechanics.

The fracture energy regularization technique is based on the assumption that dissipation takes place in a band only one element thick, irrespective of the element size. The basic concept consists on modifying the softening law in such a way that the energy dissipated over a completely degraded finite element be equal to a given value, which depends on the fracture energy of the material and on the element size. For each element, the *material characteristic length* ([13], [14]) is approximated by the *element characteristic length* l_{ch} [15], which depends on the geometric dimensions of the element and measures the computational width

of the fracture zone. The specific dissipated energy $\mathcal{D}$ is then scaled for each element so that the equation

$$\mathcal{D}\, l_{\text{ch}} = \mathcal{G}_{II} \tag{2.35}$$

holds, where $\mathcal{G}_{II}$ is the mode II fracture energy of the material, regarded to be a material property. As it is shown below, this makes the softening modulus H^p, which defines the softening response, dependent on the element size. The procedure is as follows:

For the elasto-plastic model, the rate of plastic work can be computed as:

$$\dot{\mathcal{D}} = \dot{\mathcal{W}}^p = \mathbf{s} : \dot{\mathbf{e}}^p = \widetilde{s}\, \dot{\widetilde{e}} \tag{2.36}$$

Thus, the total plastic work along a process with softening is

$$\mathcal{D} = \mathcal{W}^p = \int_{t=0}^{t=\infty} \dot{\mathcal{W}}^p dt = \int_{\xi=0}^{\xi=\infty} r^p\left(\widetilde{e}\right) \dot{\widetilde{e}} = \frac{\sigma_o^2}{2H^p} \tag{2.37}$$

It has to be remarked that the total plastic work is equal to the "area" below the $r^p - \widetilde{e}$ curve, that defines the softening response. Note also that the result in Eq. (2.37) holds both for linear and exponential softening, due to the appropriate definition of these in Box 1.

Equating the total plastic work to the energy (per unit volume) to be dissipated in the localization band, $\mathcal{W}^p = \mathcal{G}_{II}/l_{\text{ch}}$, it yields:

$$H_S^p = \frac{\sigma_o^2}{2\mathcal{G}_{II}}\, l_{\text{ch}} = \overline{H}^p\, l_{\text{ch}} \tag{2.38}$$

where $\overline{H}^p$ only depends on the material properties.

In the framework of *local* models and finite element analysis, the state variables are computed at the integration points in terms of the local strain (and/or stress) history. Therefore, the plastic internal variables r^p and $\widetilde{e}$ are defined at the integration points. The characteristic length is thus related to the volume (or area) of each finite element.

For linear simplicial elements, the characteristic length can be taken as the representative size of the element, $l_{\text{ch}} = h_e$. In this work, and assuming that the elements are equilateral, the size of the element will be computed as $h_e^2 = \left(4/\sqrt{3}\right) A_e$ for triangular elements, A_e being the area of the element, and as $h_e^3 = \left(12/\sqrt{2}\right) V_e$ for tetrahedral elements, where V_e is the volume of the element.

2.5 J_2 Viscodamage

2.5.1 Constitutive Equation

The *Continuum Damage Mechanics Theory (CDMT)* is based on the definition of the effective stress concept, which is introduced in connection with the hypothesis of strain equivalence ([16], [17], [18]): *the strain associated with a damaged state under the applied stress σ is equivalent to the strain associated with its undamaged state under the effective stress $\bar{\sigma}$.*

In the present work, the effective deviatoric stress tensor $\overline{\mathbf{s}}$ will assume the following form:

$$\overline{\mathbf{s}} = 2G\,\mathbf{e} \tag{2.39}$$

The constitutive equation for the J2-damage model is defined as:

$$p = K\varepsilon_v \tag{2.40a}$$

$$\mathbf{s} = (1-d)\,\overline{\mathbf{s}} = (1-d)\,2G\mathbf{e} \tag{2.40b}$$

where we have introduced one internal-like variable, d, the damage index, whose definition and evolution is given below.

2.5.2 Characterization of Damage

In order to clearly define concepts such as loading, unloading, or reloading for general 3D stress states, a scalar positive quantity, termed as *equivalent stress*, is defined. This allows the comparison of different 2D and 3D stress states. With such a definition, distinct 3D stress states can be mapped to a single *equivalent 1D shear test*, which makes their quantitative comparison possible [17], [18].

In the present work, the *equivalent stress* will assume the following form:

$$\tau = \sqrt{\frac{3}{2}}\,\|\overline{\mathbf{s}}\| = \sqrt{\frac{3}{2}}\,\left[\,\overline{\mathbf{s}} : \overline{\mathbf{s}}\,\right]^{1/2} \tag{2.41}$$

which corresponds to the usual definition of the equivalent von Mises stress $\widetilde{s}$.

With the above definition for the equivalent effective stress, the damage criterion, Φ^d, is introduced as:

$$\Phi^d\left(\tau, r^d\right) = \tau - r^d = \widetilde{s} - r^d \leq 0 \tag{2.42}$$

Variable r^d is an internal stress-like variable that is interpreted as the current damage threshold, in the sense that its value controls the size of the (monotonically) expanding damage surface. The initial value of the damage threshold is $r_o = \sigma_o$, where σ_o is the initial uniaxial strength.

Note that the damage criterion is defined in the effective deviatoric stress space (or, alternatively, in the deviatoric strain space). In the principal stress space, the criterion is the well-known von Mises cylinder with axis along the hydrostatic axis.

The expansion of the damage bounding surface in the normalized space for loading, unloading and reloading conditions is controlled by the Kuhn-Tucker relations and the damage consistency condition, which are

$$\dot{r}^d \geq 0 \qquad \Phi^d\left(\tau, r^d\right) \leq 0 \qquad \dot{r}^d \Phi^d\left(\tau, r^d\right) = 0 \tag{2.43a}$$

$$\text{if } \Phi^d\left(\tau, r^d\right) = 0 \text{ then } \dot{r}^d \dot{\Phi}^d\left(\tau, r^d\right) = 0 \tag{2.43b}$$

leading, in view of Eq. (2.42), to the loading condition

$$\dot{r}^d = \dot{\tau} \tag{2.44}$$

This, in turn, leads to the explicit definition of the current values of the internal variable r in the form

$$r^d = \max\left\{ r_o, \max(\tau)\right\} \tag{2.45}$$

Note that Eq. (2.45) allows to compute the current values for r^d in terms of the current value of τ, which depends explicitly on the current deviatoric strains (see Eqs. (2.39) and (2.41)).

Finally, the damage index $d = d(r^d)$ is explicitly defined in terms of the corresponding current value of the damage threshold, so that it is a monotonically increasing function such that $0 \leq d \leq 1$.

In this work, we will use the following functions:

- *Linear softening:*

$$d(r^d) = \begin{cases} \left(1 + H^d\right)\left(1 - \dfrac{r_o}{r^d}\right) & r_o \leq r^d \leq r_u = r_o\left(1 + \dfrac{1}{H^d}\right) \\ 0 & r_u \geq r^d \end{cases} \tag{2.46}$$

- *Exponential softening:*

$$d(r^d) = 1 - \frac{r_o}{r} \exp\left\{-2H^d \left(\frac{r^d - r_o}{r_o}\right)\right\} \qquad r^d \geq r_o \tag{2.47}$$

where $H^d \geq 0$ is a constant.

2.5.3 Rate dependent damage

In many materials there is a strong coupling between nonlinear rate-sensitivity and damage growth. Therefore, it is natural to develop a rate dependent constitutive model within the framework of *CDMT*, evolving from the above presented rate independent damage model, and which accounts for strain rate dependency via the damage evolution laws [7].

To this end, let us consider a viscous regularization of the rate-independent damage threshold evolution law defined by Eq. (2.44), so that Kuhn-Tucker and consistency conditions, Eqs. (2.43a) and (2.43b), of the rate independent model are replaced by the evolution law:

$$\dot{r}^d = \frac{\left\langle \Phi^d\left(\tau, r^d\right)\right\rangle}{\eta^d} = \frac{\left\langle \Phi^d\left(\tau, r^d\right)\right\rangle}{G\vartheta^d} \geq 0 \tag{2.48}$$

where $\langle\cdot\rangle$ are the Macaulay brackets (ramp function) and η^d is the damage viscosity; $\vartheta^d := \eta^d/G$ is the retardation time for damage behaviour. Notice that for very low values of the viscosity, $\eta^d \to 0$, or very small relaxation times, ϑ^d, the inviscid plastic model is recovered.

Note that this modification of the evolution law only affects the integration of the damage threshold r^d, but not the damage variable d itself. This is still obtained in a closed form, through the explicit definition of the function $d = d(r^d)$. Additionally, it is worth to remark that Eq. (2.48) guarantees monotonic increasing of the damage threshold, and, therefore, also of the damage index ($\dot{d} \geq 0$).

2.5.4 Coupling with viscoelasticy

The viscodamage model described above can be easily coupled with the viscoelastic model described in Section 2.2. To this end, the elastic definition of the effec-

tive deviatoric stresses, Eq. (2.39), is simply replaced its visco elastic counterpart

$$\overline{\mathbf{s}} = \sum_{i=0}^{N} \overline{\mathbf{s}}^i \tag{2.49}$$

where $\overline{\mathbf{s}}^i$ is the effective deviatoric stress sustained by each element of the Maxwell chain, computed as

$$\overline{\mathbf{s}}^i \;=\; \xi^i 2G(\mathbf{e} - \mathbf{e}^i) \tag{2.50}$$

where ξ^i and $\mathbf{e}^i$ are the corresponding participation ratio and viscoelastic deviatoric strain tensor, respectively.

2.5.5 Update of the damage threshold

A numerical algorithm needs to be implemented for the time integration of the damage constitutive equations presented in the previous Sections. In the following this algorithm is presented, in a strain–driven form which leads to a completely closed–form algorithm to integrate the stress tensor in time. This is most appropriate within the context of the application of the FE method.

Each time step begins at time t_n with all state variables known and it ends at time t_{n+1} with the state variables updated according to the given total strain tensor $\boldsymbol{\varepsilon}_{n+1}$. The time step size is $\Delta t = t_{n+1} - t_n$.

For the rate independent model, Eq. (2.45) allows to compute the current value for r^d_{n+1} in terms of the current value of τ_{n+1}, which in turn, depends explicitly on the current strains $\boldsymbol{\varepsilon}_{n+1}$(see Eqs. (2.39) and (2.41)). After this, the damage index $d_{n+1} = d_{n+1}\left(r^d_{n+1}\right)$ is explicitly computed in terms of the corresponding current value of the damage threshold, using the appropriate expression, Eqs. (2.46) or (2.47).

For the rate dependent model, the only difference is the updating of the damage threshold r^d_{n+1} when evolution of the damage occurs, that is, upon loading conditions. This may be evaluated using a generalized mid-point rule to integrate Eq. (2.48), i.e.,

$$r^d_{n+1} \;=\; r^d_n + \Delta r^d_{n+1} = \; r^d_n + \frac{\Delta t}{\vartheta^d} \left\langle \tau_\alpha - r^d_\alpha \right\rangle \tag{2.51}$$

where τ_α and r_α are defined by:

$$\tau_\alpha \;=\; (1-\alpha)\,\tau_n + \alpha\,\tau_{n+1} \tag{2.52a}$$

$$r^d_\alpha \;=\; (1-\alpha)\,r^d_n + \alpha\,r^d_{n+1} \tag{2.52b}$$

The choice $\alpha = 1$ Eq. (2.51) corresponds to a backward-Euler difference scheme. It is easy to show that the algorithm of Eq. (2.51) is unconditionally stable for $\alpha \geq 0.5$ and second order accurate only for $\alpha = 0.5$ (Crank-Nicholson or trapezoidal rule), which allows the use of larger time step sizes for rate-dependent analysis.

Substituting Eqs. (2.52a) and (2.52b) into Eq. (2.51), yields

$$r^d_{n+1} = \max\left\{ r^d_n, \frac{1}{1+\alpha\frac{\Delta t}{\vartheta^d}} \left[\left(1 - (1-\alpha)\frac{\Delta t}{\vartheta^d} \right) r^d_n + \frac{\Delta t}{\vartheta^d}\,\tau_\alpha \right] \right\} \tag{2.53}$$

It is worth to remark that the presented method for the integration of the damage threshold is also valid for the rate independent model, noting that for $\vartheta^d = 0$ and $\alpha = 1$, Eq. (2.53) simply reduces to the satisfaction of the monotonicity and consistency conditions

$$r^d_{n+1} = \max\left\{ r^d_n, \tau_{n+1} \right\} \tag{2.54}$$

2.5.6 Tangent operator

Rate independent damage

Differentiating Eq.(2.40b) with respect to time, we obtain

$$\dot{\mathbf{s}} = (1-d)\,\dot{\overline{\mathbf{s}}} - \dot{d}\,\overline{\mathbf{s}} \tag{2.55}$$

The effective deviatoric stresses $\overline{\mathbf{s}}$ can be computed in terms of the total strain tensor $\boldsymbol{\varepsilon}$ as

$$\overline{\mathbf{s}} = \mathbf{C}_{\text{dev}} : \boldsymbol{\varepsilon} \tag{2.56}$$

where $\mathbf{C}_{\text{dev}} = 2G\left[\,\mathbf{I} - \frac{1}{3}\,(\mathbf{1}\otimes\mathbf{1})\right]$ is the usual (fourth order) linear–elastic deviatoric constitutive tensor, $\mathbf{I}$ is the (fourth order) unit tensor and (:) denotes the tensor product contracted on two indices. Differentiating this with respect to time, we have

$$\dot{\overline{\mathbf{s}}} = \mathbf{C}_{\text{dev}} : \dot{\boldsymbol{\varepsilon}} \tag{2.57}$$

On the other hand, the time derivative of the damage index is

$$\dot{d} = d'\,\dot{r}^d \tag{2.58}$$

where the derivative $d' = d'\left(r^d\right)$ can be obtained from Eqs.(2.46)-(2.47). On loading, consistency requires that $\dot{r}^d = \dot{\tau}$, and therefore, differentiating Eq. (2.41), we can write

$$\dot{r}^d = \dot{\tau} = \frac{1}{\tau}\,\overline{\mathbf{s}} : \dot{\overline{\mathbf{s}}} = \frac{3}{2}\frac{2G}{\tau}\,\overline{\mathbf{s}} : \dot{\mathbf{e}} \tag{2.59}$$

On unloading, it is $\dot{r}^d = 0$. Substituting this result in Eq. (2.58), and the result in Eq. (2.57), yields the desired expression

$$\dot{\mathbf{s}} = \mathbf{C}^{\tan}_{\text{dev}} : \dot{\boldsymbol{\varepsilon}} \tag{2.60}$$

with

$$\left(\mathbf{C}^{\tan}_{\text{dev}}\right)^d = (1-d)\,(2G)\left[\mathbf{I} - \frac{1}{3}\,(\mathbf{1}\otimes\mathbf{1})\right]\left[\sum_{i=0}^{N}\xi^i\, e^{-\frac{\Delta t}{\vartheta^i}}\right] - h^d\,(\overline{\mathbf{s}}\otimes\overline{\mathbf{s}}) \tag{2.61}$$

where the scalar coefficient h^d is

$$h^d = \begin{cases} \dfrac{3}{2}\dfrac{2G}{\tau}\,d' & \text{for loading} \\ \\ 0 & \text{for unloading} \end{cases} \tag{2.62}$$

Rate dependent damage

In the case of rate dependent damage the determination of $\dot{r}^d$ comes from differentiating Eq. (2.51) with respect to time, to yield:

$$\dot{r}^d = \frac{\alpha\dfrac{\Delta t}{\vartheta^d}}{1+\alpha\dfrac{\Delta t}{\vartheta^d}}\;\dot{\tau} \tag{2.63}$$

Comparing Eqs. (**??**) and (2.63), it is obvious that the tangent operator for the rate dependent damage case has the same expression of Eq. (2.61) with the coefficient h^d given by

$$h^d = \begin{cases} \dfrac{\alpha\frac{\Delta t}{\vartheta^d}}{1+\alpha\frac{\Delta t}{\vartheta^d}}\,\dfrac{3}{2}\dfrac{2G}{\tau}\,d' & \text{for loading} \\ \\ 0 & \text{for unloading} \end{cases} \tag{2.64}$$

Note that for large values of $\Delta t/\vartheta^d$ the rate independent case is recovered.

2.5.7 Thermodynamic Framework

The mechanical free energy term for the damage model is defined in the form:

$$W = W_{\text{vol}}(\varepsilon_v) + (1-d)W_{\text{dev}}(\mathbf{e}) \tag{2.65a}$$

$$= \frac{1}{2} K \varepsilon_v^2 + \frac{1}{2}(1-d)\ (2G)\ \mathbf{e} : \mathbf{e} \tag{2.65b}$$

From this, and recalling that $0 \leq d \leq 1$, it is obvious that $W \geq 0$.

The constitutive equation for the damage model is obtained using Coleman's method as:

$$p = \partial_{\varepsilon_v} W = K\varepsilon_v \tag{2.66a}$$

$$\mathbf{s} = \partial_{\mathbf{e}} W = (1-d)\, 2G\mathbf{e} \tag{2.66b}$$

The mechanical dissipation can be expressed as

$$\dot{\mathcal{D}} = W^e_{\text{dev}}\, \dot{d} \quad \geq 0 \tag{2.67}$$

provided that the damage index increases monotonically, $\dot{d} \geq 0$.

2.5.8 Softening behaviour and regularization

As for the viscoplastic model, the softening behaviour must be regularized according to the characteristic lengths of the finite elements to yield meaningful results, independent of the element sizes used in the discretization. This is accomplished as follows:

Rate independent behaviour

Consider an ideal experiment in which the shear load increases *monotonically* and *quasi-statically* from an initial unstressed state to another in which full degradation takes place.

Using the rate independent version of the damage model, the specific energy dissipated in the process is:

$$\mathcal{D} = \int_{t=0}^{t=\infty} \dot{\mathcal{D}}\, dt$$

$$= \int_{t=0}^{t=\infty} W^e_{\text{dev}}\, \dot{d}\, dt$$

$$= \frac{2/3}{2\,(2G)} \int_{r=r_0}^{r=\infty} \left(r^d\right)^2 d'\, dr^d \tag{2.68}$$

where we have used Eqs. (2.67), (2.65a), (2.39), (2.41), (2.45) and the rate of damage is expressed as $\dot{d} = d' \dot{r}^d$.

We will consider in the following both the cases of linear and exponential softening:

- *Linear softening:*

  Using Eq. (2.46), $d' = (1 + H^d) r_0 / \left(r^d\right)^2$, for $r_o \leq r^d \leq r_u$, with $r_u = r_o \left(1 + 1/H^d\right)$, and $d' = 0$, otherwise. Recalling that $r_o = \sigma_o$, integrating and equating $\mathcal{D} = \mathcal{G}_{II} / l_{\text{ch}}$, we have

  $$\mathcal{D} = \left(1 + \frac{1}{H^d}\right) \frac{\sigma_o^2}{2\,(2G)} = \frac{\mathcal{G}_{II}}{l_{\text{ch}}} \tag{2.69}$$

  and, therefore,

  $$H^d = \frac{\overline{H}^d \, l_{\text{ch}}}{1 - \overline{H}^d \, l_{\text{ch}}} \qquad \geq 0 \tag{2.70}$$

  where $\overline{H}^d = \sigma_o^2 / \left(3\,(2G)\,\mathcal{G}_{II}\right)$ depends on the material properties, as $\mathcal{G}_{II}$ is the mode II fracture energy per unit area, σ_o is the uniaxial strength and G is the shear modulus.

- *Exponential softening:*

  Using now Eq. (2.47), $d' = \left(r_o + 2H^d r^d\right) \exp\left\{-2H^d \left(r^d - r\right) / r_o\right\} / r^2$, for $r^d \geq r_o$. Recalling that $r_o = \sigma_o$, and integrating, we have

  $$\mathcal{D} = \left(1 + \frac{1}{H^d}\right) \frac{\sigma_o^2}{2\,(2G)} \tag{2.71}$$

  which is identical to the result in (2.69).

Rate dependent behaviour

Let us now consider an ideal experiment in which the load increases *monotonically*, and *not quasi-statically* from an initial unstressed state to another in which full degradation takes place.

Using the rate dependent version of the model, the specific energy dissipated in the process is:

$$\begin{aligned}\mathcal{D} &= \int_{t=0}^{t=\infty} \dot{\mathcal{D}}\, dt \\ &= \int_{t=0}^{t=\infty} W^e_{\text{dev}}\ \dot{d}\, dt \\ &= \frac{2/3}{2\,(2G)} \int_{r=r_0}^{r=\infty} \left[r^d + \vartheta^d\, \dot{r}^d\right]^2 d'\, dr^d \end{aligned} \tag{2.72}$$

where we have used Eqs. (2.67), (2.65a), (2.39), and Eq. (2.48) and the rate of damage is expressed as $\dot{d} = d'\, \dot{r}^d$.

Comparing Eq. (2.72) with Eq. (2.68) it is obvious that the first one reduces to the second for a null value of ϑ^d, or for very slow processes, with $\dot{r}^d \to 0$.

In other cases, the evolution law, Eq. (2.48), ensures that the terms r^d and $\vartheta^d\, \dot{r}^d$ are of the same order, that is $\left(\vartheta^d\, \dot{r}^d / r^d\right) = \mathcal{O}(1)$. Therefore, it can be assumed that the regularized parameter from Eq. (2.70), will also regularize the rate dependent model, both for linear and exponential softening.

2.6 Overlay J_2 Viscoelasto-Viscoplastic-Viscodamage model

It is obvious from the above discussion that softening behaviour can be modelled either via a (visco)plastic or a (visco)damage model. If appropriate material data is supplied, both models would render the same stress vs. strain behaviour when monotonically increasing straining is applied. However, the internal performance and dissipative mechanisms of both models is rather different. The different essence of the models is displayed upon unloading: (visco)plastic models unload (visco)elastically, with evident permanent plastic deformation; on the other hand, (visco)damage models unload secantly, with evident permanent loss of stiffness.

The behaviour of real materials may follow complex loading and unloading stress vs. strain curves, exhibiting both permanent inelastic strains and loss of stiffness. This is why many models have been proposed in the literature to combine the features of plastic and damage models ([17], [18], [19], [20], [21], among others).

In this work, we propose to combine them in the most simple, and efficient, manner, constructing an *overlay* model, that can be rigorously based in *Mixing*

Theory ([22], [23]), used in the last decades to appropriately model composite materials such as concrete ([24], [25], [26], [27]). It has to be remarked that Mixing Theory was originally conceived precisely to achieve the goal here pursued: the proper combination of features of different material models.

The basic assumption of the overlay model is that the plastic and damage dissipative mechanisms work *in parallel*, that is, that they are subjected to the same total strains. Therefore, for a J_2 overlay plastic-damage model, we can define the mechanical free energy in the form

$$W^e = W_{\rm vol}(\varepsilon_v) + (1-\beta)\,(W_{\rm dev}(\mathbf{e}^e))^p + \beta\,(W_{\rm dev}(\mathbf{e}))^d \tag{2.73a}$$

$$= \frac{1}{2}\,K\,\varepsilon_v^2 + \frac{(1-\beta)}{2}\,(2G)\,(\mathbf{e}-\mathbf{e}^p):(\mathbf{e}-\mathbf{e}^p) + \frac{\beta}{2}(1-d)\,(2G)\,\mathbf{e}:\mathbf{e} \tag{2.73b}$$

where β is a material parameter that determines the ratio of participation of the damage and plastic "components" of the material. Note that for $\beta = 0$ and $\beta = 1$ the purely plastic and damage models are obtained as limit cases. It is obvious that this definition can incorporate viscoelastic behaviour in a natural fashion.

The constitutive equations for the overlay model are obtained using Coleman's method as:

$$p = \partial_{\varepsilon_v} W = K\varepsilon_v \tag{2.74a}$$

$$\mathbf{s} = \partial_{\mathbf{e}}\, W = 2G\,[(1-\beta)\mathbf{e}^e + \beta\,(1-d)\,\mathbf{e}] \tag{2.74b}$$

The tangent operator is, evidently,

$$\mathbf{C}^{\rm tan}_{\rm dev} = (1-\beta)\left(\mathbf{C}^{\rm tan}_{\rm dev}\right)^p + \beta\left(\mathbf{C}^{\rm tan}_{\rm dev}\right)^d \tag{2.75}$$

where $(\mathbf{C}^{\rm tan}_{\rm dev})^p$ and $(\mathbf{C}^{\rm tan}_{\rm dev})^d$ are defined by Eqns. (2.31) and (2.61), respectively.

3 Boundary value problem

3.1 Strong and weak forms

The strong form of the continuum mechanical problem can be stated as: find the displacement field $\mathbf{u}$ and the pressure field p, for given prescribed body forces $\mathbf{f}$, such that:

$$\nabla \cdot \mathbf{s} + \nabla p + \mathbf{f} = \mathbf{0} \qquad \text{in } \Omega \tag{3.1a}$$

$$\nabla \cdot \mathbf{u} - \frac{1}{K} p = 0 \qquad \text{in } \Omega \tag{3.1b}$$

where Ω is the open and bounded domain of $\mathbb{R}^{n_{\text{dim}}}$ occupied by the solid in a space of n_{dim} dimensions. Eqs. (3.1a)-(3.1b) are subjected to appropriate Diritchlet and Neumann boundary conditions. In the following, we will assume these in the form of prescribed displacements $\mathbf{u} = \overline{\mathbf{u}}$ on $\partial\Omega_u$, and prescribed tractions $\overline{\mathbf{t}}$ on $\partial\Omega_t$, respectively. In the mixed formulation the value of the pressure is defined by the Neumann conditions or, alternatively, by prescribing its value at some point.

The associated weak form of the problem (3.1a)+(3.1b) can be stated as:

$$(\mathbf{v}, \nabla \cdot \mathbf{s}) + (\mathbf{v}, \nabla p) + (\mathbf{v}, \mathbf{f}) = 0 \qquad \forall \mathbf{v} \tag{3.2a}$$

$$(q, \nabla \cdot \mathbf{u}) - \left(q, \frac{1}{K} p\right) = 0 \qquad \forall q \tag{3.2b}$$

where $\mathbf{v} \in \mathcal{V}$ and $q \in \mathcal{Q}$ are the variations of the displacements and pressure fields, respectively, $\mathcal{V} = H_0^1(\Omega)$ is the space of continuous functions with discontinuous derivatives, $\mathcal{Q} = L^2(\Omega)$ is the space of square integrable functions in Ω and $(\cdot, \cdot)$ denotes the inner product in $L^2(\Omega)$. Integrating Eq. (3.2a) by parts, the problem can be rewritten in the standard form as:

$$(\nabla^s \mathbf{v}, \mathbf{s}) + (\nabla \cdot \mathbf{v},\, p) - (\mathbf{v}, \mathbf{f}) - \left(\mathbf{v}, \overline{\mathbf{t}}\right)_{\partial\Omega} = 0 \qquad \forall \mathbf{v} \tag{3.3a}$$

$$(q, \nabla \cdot \mathbf{u}) - \left(q, \frac{1}{K} p\right) \;=\; 0 \qquad \forall q \tag{3.3b}$$

3.2 Irreductible, mixed and stabilized methods

Over the last years, many researchers have supported the misleading idea that the underlying reason why the standard, local, rate-independent constitutive models are inadequate to model zones of localized straining correctly is the local change of character of the governing equations (see [28], [29], [30], [31], [32], [33], [34], [35], [36], [34], [37] and many others.).

In fact, substituting Eq. (3.1b) into Eq. (3.1a), and reducing the discussion to standard elasticity, yields the irreductible form:

$$G\Delta\mathbf{u} + K\nabla\left(\nabla \cdot \mathbf{u}\right) + \mathbf{f} = \mathbf{0} \qquad \text{in } \Omega \tag{3.4}$$

where $\Delta\left(\cdot\right)$ denotes the laplacian operator and G and K are the shear and bulk modulus, respectively.

A standard stability (or energy) estimate for problem (3.4) is obtained by multiplying the left hand side by $\mathbf{u}$ and integrating by parts over the domain Ω, to yield

$$G\left(\nabla\mathbf{u},\nabla\mathbf{u}\right) + K\left(\nabla \cdot \mathbf{u},\nabla \cdot \mathbf{u}\right) = G\left\|\nabla\mathbf{u}\right\|^2 + K\left\|\nabla \cdot \mathbf{u}\right\|^2 = \left\|\mathbf{u}\right\|_E^2 \tag{3.5}$$

where $\left\|\cdot\right\|_E^2$ is the energy norm (equal to the elastic free energy). From Eqs. (**??**)-(**??**), the elliptic character of the original equations is evident, for $G, K \geq 0$. It is, therefore, obvious that in nonlinear solid continuum mechanics *with softening*, where the local *tangent* values of the moduli become negative, the *rate* equations lose ellipticity. It is important to note that as long as the *secant* moduli remain positive, the equations in terms of the total displacement $\mathbf{u}$ (non its increments) remain elliptic.

Anyway, loss of ellipticity *does not* mean that the problem be ill-posed or that it can not be solved numerically. Parabolic and hyperbolic partial differential equations certainly have solutions and they can be computed, analytically or numerically.

The true panorama is as follows. For a *compressible irreductible elliptic problem in the continuum*, it can be proved that the solution $\mathbf{u} \in \mathcal{V}$ exists and it is unique, $\mathcal{V}$ being the appropriate functional space. It can also be proved that,

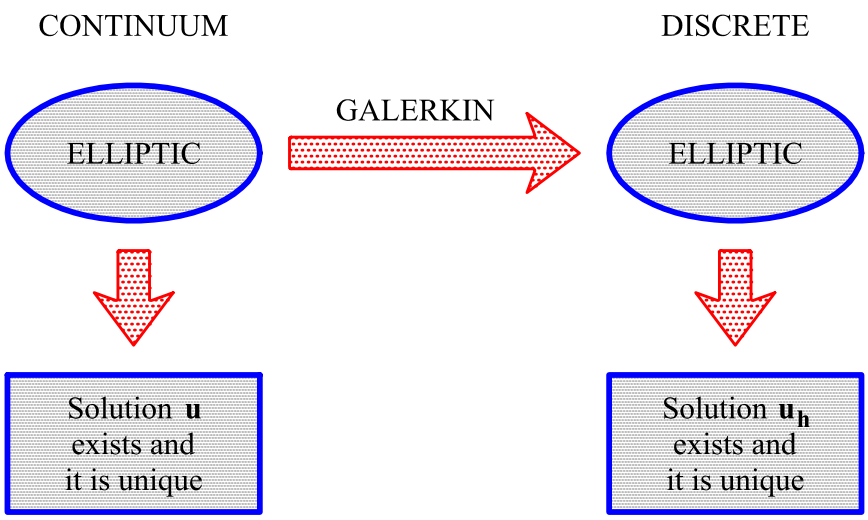

Fig. 3.1: Continuum and discrete compressible irreductible elliptic *problem*

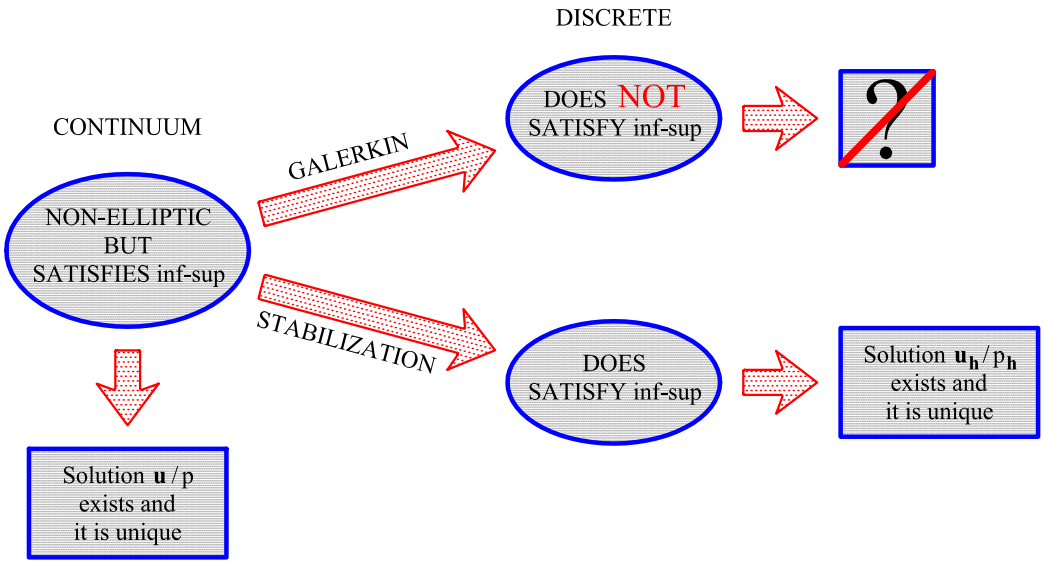

Fig. 3.2: Continuum and discrete incompressible mixed non-elliptic *problem*

for this problem, the standard Galerkin discretization method provides a *discrete irreductible problem* which inherits the elliptic nature of the original problem. Therefore, the discrete solution $\mathbf{u}_h \in \mathcal{V}_h$ exists and it is unique, $\mathcal{V}_h$ being an appropriate finite element functional space. This situation is depicted in Figure 3.1.

The situation is more complex when incompressibility takes places in the domain. Let us now consider a *mixed problem in the continuum* with some incompressibility constraint present, either globally or locally. It can be proved that a solution $\mathbf{u} \in \mathcal{V}$, $p \in \mathcal{Q}$ exists and it is unique if the spaces $\mathcal{V}$ and $\mathcal{Q}$ satisfy the *inf-sup* condition [38]. Unfortunately, satisfaction of the *necessary and sufficient inf-sup* condition is not necessarily inherited by the corresponding discrete problem. For instance, if we attempt to solve the incompressible problem using standard simplexes, such as constant strain triangles or tetrahedra, we have $\mathcal{V} = P_1$ and $\mathcal{Q} = P_0$, which *do not* satisfy the *inf-sup* condition. This, and not the loss of ellipticity is the reason why the standard irreductible formulation fails miserably when attempting to solve localization problems. Figure 3.2 illustrates the explained situation for these problems.

It is, therefore, evident that the origin of the difficulties encountered when attempting to solve incompressible problems with non-stable finite element formulations does not lay on the local format of the constitutive equations, as many reputed researchers have assured during the last decade, but on the inadequacy of the discretization method used. It is also very clear that to solve localization problems it is necessary to use a discretization procedure that satisfies the *necessary and sufficient inf-sup* condition. In the following, we propose the use of the *orthogonal sub-grid scale stabilization method (OSGS)* to solve this type of problems.

3.3 The Sub-Grid Scale approach

The *discrete* finite element form of the problem is obtained from Eqs. (3.3a)-(3.3b), substituting the displacement and pressure fields and their variations by their standard finite element interpolations:

$$(\nabla^s \mathbf{v}_h, \mathbf{s}_h) + (\nabla \cdot \mathbf{v}_h,\, p_h) - (\mathbf{v}_h, \mathbf{f}) - \left(\mathbf{v}_h, \overline{\mathbf{t}}\right)_{\partial\Omega} = 0 \qquad \forall \mathbf{v}_h \qquad (3.6a)$$

$$(q_h, \nabla \cdot \mathbf{u}_h) - \left(q_h, \frac{1}{K} p_h\right) = 0 \qquad \forall q_h \qquad (3.6b)$$

where $\mathbf{u}_h$, $\mathbf{v}_h \in \mathcal{V}_h$ and p_h , $q_h \in \mathcal{Q}_h$ are the *discrete* displacement and pressure fields and their variations, defined onto the finite element spaces $\mathcal{V}_h$ and $\mathcal{Q}_h$, respectively.

As it is well known, the inf-sup condition [38], poses severe restrictions on the choice of the spaces $\mathcal{V}_h$ and $\mathcal{Q}_h$ when using the standard Galerkin discrete form (3.6a)-(3.6b). For instance, standard mixed elements with continuous equal order linear/linear interpolation for both fields are not stable, and the lack of stability shows as uncontrollable oscillations in the pressure field that usually, and very particularly in non linear problems, pollute the solution entirely. Fortunately, the strictness of the inf-sup condition can be circumvented by modifying the discrete variational form appropriately, in order to attain the necessary stability with the desired choice of interpolation spaces.

The basic idea of the sub-grid scale approach [39] is to consider that the continuous displacement field can be split in two components, one coarse and a finer one, corresponding to different scales or levels of resolution. The solution of the continuous problem contains components from both scales. For the solution of the discrete problem to be stable it is necessary to, somehow, include the effect of both scales in the approximation. The coarse scale can be appropriately solved by a standard finite element interpolation, which however cannot solve the finer scale. Nevertheless, the effect of this finer scale can be included, at least locally, to enhance the stability of the pressure in the mixed formulation.

To this end, the displacement field of the mixed problem will be approximated as

$$\mathbf{u} = \mathbf{u}_h + \widetilde{\mathbf{u}} \tag{3.7}$$

where $\mathbf{u}_h \in \mathcal{V}_h$ is the displacement component of the (coarse) finite element scale and $\widetilde{\mathbf{u}} \in \widetilde{\mathcal{V}}$ is the enhancement of the displacement field corresponding to the (finer) sub-grid scale. Let us also consider the corresponding variations $\mathbf{v}_h \in \mathcal{V}_h$ and $\widetilde{\mathbf{v}} \in \widetilde{\mathcal{V}}$, respectively. This extends the displacement solution space to $\mathcal{V} \simeq \mathcal{V}_h \oplus \widetilde{\mathcal{V}}$.

It is reasonable to assume that the sub-grid displacements $\widetilde{\mathbf{u}}$ will be sufficiently "small" compared to $\mathbf{u}_h$; they can be viewed as a "high frequency" perturbation of the finite element field, which cannot be resolved in $\mathcal{V}_h$. It can also be assumed that $\widetilde{\mathbf{u}}$ and $\widetilde{\mathbf{v}}$ vanish on the boundary $\partial\Omega$. It must be pointed out that no sub-grid scale contribution has been considered on the pressure field.

Considering the subscales, the deviatoric stresses can be decomposed into two

different contributions

$$\mathbf{s}(\mathbf{u}) = \mathbf{s}_h(\mathbf{u}) + \widetilde{\mathbf{s}}(\mathbf{u}) \tag{3.8}$$

Notice that the stresses $\mathbf{s}$ are *not* a linear function of $\mathbf{u}$ and, therefore, it is *not exactly true* that $\mathbf{s}_h = \mathbf{s}_h(\mathbf{u}_h)$ and $\widetilde{\mathbf{s}} = \widetilde{\mathbf{s}}(\widetilde{\mathbf{u}})$. However, we can approximate the stresses corresponding to the coarse finite element scale in the standard fashion, as:

$$\mathbf{s}_h(\mathbf{u}) \cong \mathbf{s}_h(\mathbf{u}_h) = 2G^*\mathbf{e}_h \tag{3.9}$$

which can be computed following the integration algorithm proposed in the next chapter. In Eq. (3.9) we have introduced the *secant* shear modulus as (half) the ratio between the norms of the deviatoric stress and *total* strain tensors, $2G^* = \|\mathbf{s}_h\| / \|\mathbf{e}_h\|$. For non-linear constitutive models, this ratio is obviously non-constant and it varies along the deformation process.

Being the enhancement $\widetilde{\mathbf{u}}$ "small" compared to $\mathbf{u}_h$, it is possible to make the following approximation for the strains due to the sub-scale:

$$\frac{\|\widetilde{\mathbf{s}}\|}{\|\widetilde{\mathbf{e}}\|} \cong \frac{\|\mathbf{s}_h\|}{\|\mathbf{e}_h\|} = 2G^* \tag{3.10}$$

which motivates the approximation:

$$\widetilde{\mathbf{s}}(\mathbf{u}) \cong \widetilde{\mathbf{s}}(\widetilde{\mathbf{u}}) = 2G^*\widetilde{\mathbf{e}} \tag{3.11}$$

It can be remarked that the formalism of approximation (3.11) holds for other non-linear constitutive models, such as nonlinear elasticity or plasticity.

With these definitions, the discrete problem corresponding to Eqs. (3.2a) and (3.2b) is now:

$$\begin{aligned}
(\nabla^s\mathbf{v}_h, \mathbf{s}_h) + \boxed{(\nabla^s\mathbf{v}_h, \widetilde{\mathbf{s}})} + (\nabla\cdot\mathbf{v}_h,\, p_h) & \\
- (\mathbf{v}_h, \mathbf{f}) - \left(\mathbf{v}_h, \overline{\mathbf{t}}\right)_{\partial\Omega_t} &= 0 \qquad \forall\mathbf{v}_h \qquad (3.12a)\\
(\widetilde{\mathbf{v}}, \nabla\cdot\mathbf{s}_h) + (\widetilde{\mathbf{v}}, \nabla\cdot\widetilde{\mathbf{s}}) + (\widetilde{\mathbf{v}}, \nabla p_h) + (\widetilde{\mathbf{v}}, \mathbf{f}) &= 0 \qquad \forall\widetilde{\mathbf{v}} \qquad (3.12b)\\
(q_h, \nabla\cdot\mathbf{u}_h) - \left(q_h, \frac{1}{K}p_h\right) + \boxed{(q_h, \nabla\cdot\widetilde{\mathbf{u}})} &= 0 \qquad \forall q_h \qquad (3.12c)
\end{aligned}$$

where Eq. (3.12a) has been integrated by parts, recalling that $\widetilde{\mathbf{u}}$ and $\widetilde{\mathbf{v}}$ vanish on the boundary.

Due to the approximation used, Eq. (3.7), and the linear independence of $\mathbf{v}_h$ and $\widetilde{\mathbf{v}}$, Eq. (3.7), now the continuum Eq. (3.3b) unfolds in two discrete equations,

one related to each scale considered. Equations (3.12a) and (3.12c) are defined in the finite element spaces $\mathcal{V}_h$ and $\mathcal{Q}_h$, respectively. The first one solves the balance of momentum including a stabilization term $\mathsf{S}_1 = (\nabla^s \mathbf{v}_h, \widetilde{\mathbf{s}})$ depending on the sub-grid stresses $\widetilde{\mathbf{s}}$. The second one enforces the incompressibility condition including a stabilization term $\mathsf{S}_2 = (q_h, \nabla \cdot \widetilde{\mathbf{u}})$ depending on the sub-grid displacements $\widetilde{\mathbf{u}}$. On the other hand, equation (3.12b) is defined in the sub-grid scale space $\widetilde{\mathcal{V}}$ and, hence, it cannot be solved by the finite element mesh. Let us now rewrite Eq. (3.12b) in the form:

$$-(\widetilde{\mathbf{v}}, \nabla \cdot \widetilde{\mathbf{s}}) = (\widetilde{\mathbf{v}}, \mathbf{r}_h) \qquad \forall \widetilde{\mathbf{v}} \in \widetilde{\mathcal{V}} \tag{3.13}$$

where the residual of the Cauchy equation in the finite element scale is defined as:

$$\mathbf{r}_h = \mathbf{r}_h(\mathbf{u}_h, p_h) = \nabla \cdot \mathbf{s}_h + \nabla p_h + \mathbf{f} \tag{3.14}$$

Now, some appropriate approximations are necessary. According to hypotheses (3.10) and (3.11), let us assume that, within each finite element Ω_e,

$$\|\nabla \cdot \widetilde{\mathbf{s}}\| \cong \frac{\|\widetilde{\mathbf{s}}\|}{c_1 h_e} = \frac{2G_e^* \|\widetilde{\mathbf{e}}\|}{c_1 h_e} \cong \frac{2G_e^*}{c_1 h_e}\left(\frac{\|\widetilde{\mathbf{u}}\|}{c_2 h_e}\right) = \frac{1}{\tau_e}\|\widetilde{\mathbf{u}}\| \tag{3.15}$$

where the parameter $\tau_e = ch_e^2/2G_e^*$ is defined as a function of the characteristic length of the element h_e and the current secant shear modulus G_e^*. The constant $c = c_1 c_2 = \mathcal{O}(1)$ has to be determined through numerical testing. This very simple and heuristic approximation of the *effect of the sub-scale* is one of the keys to the success of the stabilization procedure of the incompressible problem. More elaborated assumptions may be needed in other situations.

Integrating the stabilization terms by parts, and recalling that the subscale displacements vanish on the boundary, it yields

$$\mathsf{S}_1 = (\nabla^s \mathbf{v}_h, \widetilde{\mathbf{s}}) = -(\widetilde{\mathbf{u}}, \nabla \cdot (2G^* \mathrm{dev}\ \nabla^s \mathbf{v}_h)) \tag{3.16a}$$

$$\mathsf{S}_2 = (q_h, \nabla \cdot \widetilde{\mathbf{u}}) = -(\widetilde{\mathbf{u}}, \nabla q_h) \tag{3.16b}$$

The term $\nabla \cdot (\mathrm{dev}\ \nabla^s \mathbf{v}_h)$ in (3.16a) involves second derivatives of finite element functions which vanish when linear elements are used. In the case of higher order elements these derivatives can be neglected, leading to a method which is still consistent, but with a non-optimal rate of convergence [41].

3.4 Orthogonal Sub-Grid Scales (OSGS) and Galerking Least Squares (GLS) stabilizations

The objective in this section is to obtain a useful expression for the sub-grid scale displacements $\widetilde{\mathbf{u}}$ to be introduced in the stabilization term S_2 in Eq. (3.12c).

It was argued in [47] that a very *natural* choice for the unknown subgrid space $\widetilde{\mathcal{V}}$ is the space orthogonal to the finite element space, referred to hereafter as $\mathcal{V}_h^{\perp}$. This means approximating the displacement solution space as $\mathcal{V} \simeq \mathcal{V}_h \oplus \mathcal{V}_h^{\perp}$. The subsequent stabilization method is called *orthogonal* sub-grid scale method, and it has already been successfully applied to several problems in fluid mechanics.

Also, the format of the Eq. (3.13), which is *exact* for the fine scale and *nonlocal*, strongly suggests that $\nabla \cdot \widetilde{\mathbf{s}}$, and hence $\widetilde{\mathbf{u}}$, are *driven* by the residual of the coarse scale, $\mathbf{r}_h$. In [40] it is reasoned that the sought effect of the finer scale is to explicitly account for the *distributional effects* of the residual of the coarse scale.

Because of these two reasons, we will take $\widetilde{\mathbf{v}} \in \mathcal{V}_h^{\perp}$, and assume that

$$-\left(\widetilde{\mathbf{v}}, \nabla \cdot \widetilde{\mathbf{s}}\right) \cong \left(\widetilde{\mathbf{v}}, P_h^{\perp}\left(\mathbf{r}_h\right)\right) \qquad \forall \widetilde{\mathbf{v}} \in \mathcal{V}_h^{\perp} \tag{3.17}$$

where $P_h^{\perp}(\mathbf{x})$ is the orthogonal projection of $\mathbf{x}$ onto $\mathcal{V}_h^{\perp}$, which can be expressed as $P_h^{\perp}(\mathbf{x}) = \mathbf{x} - P_h(\mathbf{x})$. The L^2 projection of $\mathbf{x}$ onto the finite element space, or *least square fitting*, can easily be computed from the orthogonality condition

$$\left(P_h(\mathbf{x}) - \mathbf{x}\ ,\ \boldsymbol{\eta}_h\right) = 0 \qquad \forall \boldsymbol{\eta}_h \in \mathcal{V}_h \tag{3.18}$$

Using approximations (3.15) and (3.17), the sub-scale displacements can be *localized* within each finite element Ω_e, and be expressed as

$$\widetilde{\mathbf{u}}_e = \tau_e\, P_h^{\perp}\left(\mathbf{r}_h\right) \quad \in \mathcal{V}_h^{\perp} \tag{3.19}$$

where the positive sign is necessary from stability considerations.

Some remarks are in order:

1. As expected, $\widetilde{\mathbf{u}}$ is sufficiently "small" compared to $\mathbf{u}_h$ ($\widetilde{\mathbf{u}} \simeq \mathcal{O}(h^2)$).

2. With this definition, $\widetilde{\mathbf{u}}$ is discontinuous across element boundaries. For linear elements, $\widetilde{\mathbf{u}}$ is piece-wise linear.

3. Even if defined element-wise, $\widetilde{\mathbf{u}}_e$ cannot be condensed at element level, because $P_h^{\perp}(\cdot)$ is a global operator.

4. In the localization process, it is necessary to neglect the integrals over element faces involving the sub-scale, in front of the integrals over the element volumes. This is justified in [41] resorting to Fourier analysis and recalling that the subscale is associated to higher frequencies that the grid scale. It is worth to mention that for "bubble"-type enhancements these boundary terms are null by construction [42], [43].

5. Eq. (3.19) does not need to be interpreted *point-wise,* as the values of $\widetilde{\mathbf{u}}$ are not used in the stabilization procedure; only the integrals S_1 and S_2 in Eqs. (3.16a)-(3.16b) are needed.

It must be pointed out that $\mathbf{f}$ in (3.14) can be assumed to belong to the space $\mathcal{V}_h$ and, consequently, $P_h^{\perp}(\mathbf{f}) = \mathbf{0}$. Also, $\nabla\cdot\mathbf{s}_h$ in (3.14) involves second derivatives of finite element functions which vanish when linear elements are used. Taking all this into account, expression (3.19) transforms in

$$\widetilde{\mathbf{u}}_e = \tau_e \ (\nabla p_h - P_h(\nabla p_h)) \tag{3.20}$$

Finally, substituting Eq. (3.20) into the expression of the stabilization term S_2, see Eq. (3.16b), it simplifies as

$$\mathsf{S}_2 = -\sum_{e=1}^{n_{elm}} \tau_e \ (\nabla q_h \cdot [\nabla p_h - P_h(\nabla p_h)]) \tag{3.21}$$

Observe that this stabilization term is computed in an element by element manner and, within each element, its magnitude depends on the difference between the continuous (projected) and the discontinuous (elemental) pressure gradient. This means that the term added to secure a stable solution decreases very rapidly upon mesh refinement, as the finite element scale becomes finer and the *projection of the residual* reduces. This happens at a greater rate than with other stabilization techniques, such as the Galerkin Least Square (GLS) method, where the stabilization terms are proportional to the *residual itself ,* see [44], [45] and below.

The projection of the pressure gradient onto the finite element space $\mathcal{V}_h$, $\mathbf{\Pi}_h = P_h(\nabla p_h)$, is computed as:

$$(\nabla p_h \ , \ \boldsymbol{\eta}_h) = (\mathbf{\Pi}_h, \ \boldsymbol{\eta}_h) \qquad \forall \boldsymbol{\eta}_h \in \mathcal{V}_h \tag{3.22}$$

As a result of the above procedure, the stabilized mixed system of equations proposed in this work to solve the problem of incompressible elasto-damage behavior with linear/linear interpolations for the displacement and pressure fields is the following:

$$(\nabla^s \mathbf{v}_h, \mathbf{s}_h) + (\nabla \cdot \mathbf{v}_h, p_h) - (\mathbf{v}_h, \mathbf{f}) - \left(\mathbf{v}_h, \overline{\mathbf{t}}\right)_{\partial\Omega_t} = 0 \qquad \forall \mathbf{v}_h \quad (3.23a)$$

$$(q_h, \nabla \cdot \mathbf{u}_h) - \left(q_h, \frac{1}{K} p_h\right) - \sum_{e=1}^{n_{elm}} \tau_e \ (\nabla q_h \cdot [\nabla p_h - \mathbf{\Pi}_h]) = 0 \qquad \forall q_h \quad (3.23b)$$

$$(\nabla p_h \ , \ \boldsymbol{\eta}_h) - (\mathbf{\Pi}_h, \ \boldsymbol{\eta}_h) = 0 \qquad \forall \boldsymbol{\eta}_h \quad (3.23c)$$

It is important to point out that, when using linear/linear displacement and pressure interpolations, the only stabilization term appears in the incompressibility equation (3.23b), see [1], [2], [3], [4], [5]. Observe that in it, the third nodal variable $\mathbf{\Pi}_h$ is not other that the L_2_projection (least square fitting) of the pressure gradient, $\mathbf{\Pi}_h = P_h(\nabla p_h)$. The next section shows that the drawback of accounting for an extra nodal variable can be easily overcome to achieve a robust and efficient procedure.

An alternative stabilization method is the one known as *Galerkin Least Square (GLS)*, originally proposed in [44]. The corresponding *stabilized discrete problem* reads:

$$(\nabla^s \mathbf{v}_h, \mathbf{s}_h) + (\nabla \cdot \mathbf{v}_h, p_h) - (\mathbf{v}_h, \mathbf{f}) - \left(\mathbf{v}_h, \overline{\mathbf{t}}\right)_{\partial\Omega_t} = 0 \qquad \forall \mathbf{v}_h \quad (3.24a)$$

$$(q_h, \nabla \cdot \mathbf{u}_h) - \left(q_h, \frac{1}{K} p_h\right) - \boxed{\sum_{e=1}^{n_{elm}} \tau_e \ (\nabla q_h \cdot \nabla p_h)} = 0 \qquad \forall q_h \quad (3.24b)$$

which has a format very similar to the OSGS method, but does not require the computation of any extra nodal variable. Experience shows that the GLS method is more diffusive that the OSGS stabilization. This means that GLS is somewhat more "robust" than OSGS, but sometimes less sharp localizations are obtained.

3.5 Stabilization parameter

The stabilization techniques discussed in the previous section are designed to provide stability to the incompressible elasto-damage problem. In reference [3]

it was found that, with perfect plasticity, the stabilization parameter has to be modified to account for the development of the plastic regime, as deformation localizes into weak discontinuities; otherwise, pressure oscillations arise in the vicinity of the damaged areas and pollute the solution. In [3], it was proposed to enhance the stabilization properties using a *nonlinear* stabilization parameter

$$\tau_e = \frac{ch_e^2}{2G^*} \tag{3.25}$$

computed as a function of the characteristic length of the element h_e and the current *secant* shear modulus G^*, defined as (half) the ratio between the norms of the deviatoric stress and *total* strain tensors, $2G^* = \|\mathbf{s}\| / \|\mathbf{e}\|$. The constant $c = \mathcal{O}(1)$ has to be determined through numerical testing.

For nonlinear constitutive models, this ratio is obviously non-constant and it varies along the deformation process. In the softening regime, it is clear that, as deformation evolves, the secant modulus G^* decreases and, consequently, the value of τ_e increases, further relaxing the incompressibility constraint.

3.6 Consistent residual viscosity

For J_2-softening materials, shear strain localizes and the modulus G^* decreases very fast with increasing deformation and, ultimately, vanishes, yielding very large values of the stabilization parameter. At the same time, the components of the tangent deviatoric constitutive tensor diminish, eventually leading to a non-positive definite global stiffness matrix. It is found that these circumstances cause numerical difficulties that translate in slow or even lack of convergence of the solution of the nonlinear discrete equations, particularly in problems involving singular points, where the strains reach very large values.

Therefore, it is necessary to enhance the convergence properties of the nonlinear equilibrium iterations. In this work, we use the *consistent residual viscous regularization* proposed in [4] and [5]. This consists on using a residual artificial viscosity defined in terms of the orthogonal projection of the residual of the momentum equation onto the finite element space, in the form

$$\vartheta^r = c' \frac{h_e \Delta t}{G} \|\nabla p_h - \mathbf{\Pi}_h\| \tag{3.26}$$

where $c' = \mathcal{O}(1)$ is a constant, h_e is the characteristic length of the element, Δt

is the time step size and σ_o is the uniaxial strength. Note that as it is defined, ϑ^r has units of time.

This residual viscosity acts only in those elements where the momentum equation is not exactly satisfied and that, for linear simplex, it is $\vartheta^r = \mathcal{O}\left(h_e^2 \Delta t\right)$. This means that it maintains the order of the finite element approximation, as it vanishes upon mesh (and time increment) refinement with the appropriate rate. The structure of expression (3.26) suggests that it is also possible to define the viscosity purely in terms of the norm of the pressure gradient, in the form

$$\vartheta^r = c' \frac{h_e \Delta t}{G} \|\nabla p_h\| \tag{3.27}$$

This second proposal is consistent with the definition of the stabilization term used in the original GLS method.

In the numerical examples showed below, the *effective* plastic and damage viscosities, $\overline{\vartheta}^p$and $\overline{\vartheta}^d$ are taken, for each element, as

$$\overline{\vartheta}^p = \max\left(\vartheta^p, \vartheta^r\right) \tag{3.28a}$$

$$\overline{\vartheta}^d = \max\left(\vartheta^d, \vartheta^r\right) \tag{3.28b}$$

where ϑ^p and ϑ^d are the corresponding plastic and damage *material* viscosities, respectively, and ϑ^r is the residual viscosity.

It is well known that "viscosity", i.e. rate-dependent nonlinear behaviour is one of the ways to preserve the elliptic character of the mechanical problem [48]. It must be emphasized that, in this work, the objective of the use of the residual regularization is *not* this preservation, but the enhancement of convergence.

3.7 Implementation and computational aspects

Due to the nonlinear dependence of the stresses on the displacements, the solution of the system of equations (3.23a)-(3.23c) requires the use of an appropriate incremental/iterative procedure such as the Newton-Raphson method. Within such a procedure, the system of linear equations to be solved for the $(i+1)$-th equilibrium iteration of the $(n+1)$-th time (or load) step is:

$$\begin{bmatrix} \mathbf{K}_{\text{dev}} & \mathbf{G} & \mathbf{0} \\ \mathbf{G}^T & -\left(\frac{1}{K}\mathbf{M} + \mathbf{L}_{\boldsymbol{\tau}}\right) & \mathbf{G}_{\boldsymbol{\tau}}^T \\ \mathbf{0} & \mathbf{G}_{\boldsymbol{\tau}} & -\mathbf{M}_{\boldsymbol{\tau}} \end{bmatrix}^{(n+1,i)} \begin{bmatrix} \delta\mathbf{U} \\ \delta\mathbf{P} \\ \delta\boldsymbol{\Pi} \end{bmatrix}^{(n+1,i+1)} = - \begin{bmatrix} \mathbf{R}_1 \\ \mathbf{R}_2 \\ \mathbf{0} \end{bmatrix}^{(n+1,i)} \tag{3.29}$$

where $\delta\mathbf{U}$, $\delta\mathbf{P}$ and $\delta\mathbf{\Pi}$ are the iterative corrections to the nodal values for the displacements, pressure and pressure gradient, respectively, $\mathbf{R}_1$ and $\mathbf{R}_2$ are the residual vectors associated to the satisfaction of the balance of momentum and incompressibility equations, respectively, and the *global* matrices $\mathbf{K}_{\text{dev}}, \mathbf{G}, \mathbf{G}_{\boldsymbol{\tau}}, \mathbf{M}, \mathbf{L}_{\boldsymbol{\tau}}$ and $\mathbf{M}_{\boldsymbol{\tau}}$ come from the standard assembly procedure of the elemental contributions, for the i-th iteration of the $n+1$ step. Note that this global matrix is symmetric, but it is not positive definite. Each one of the elemental matrices $\mathbf{K}^{(e)}$ has the *symmetric* structure:

$$\left[\mathbf{K}^{AB}\right]^{(e)} = \begin{bmatrix} \mathbf{K}^{AB}_{\text{dev}} & \mathbf{G}^{AB} & \mathbf{0} \\ \left(\mathbf{G}^{AB}\right)^T & -\tau_e L^{AB} & \tau_e \left(\mathbf{G}^{AB}\right)^T \\ \mathbf{0} & \tau_e \mathbf{G}^{AB} & -\tau_e \, \mathbf{M}^{AB} \end{bmatrix}^{(e)} \tag{3.30}$$

where the entry $(\cdot)^{AB}$ is a sub-matrix corresponding to the local nodes A and B. In equation (3.30), $\mathbf{K}^{AB}_{\text{dev}}$ is the deviatoric component of the standard elasto-damaged tangent stiffness matrix defined as:

$$\mathbf{K}^{AB}_{\text{dev}} = \int_{\Omega_e} \mathbf{B}^T_A \mathbf{D}^{ep}_{\text{dev}} \mathbf{B}_B \, d\Omega \tag{3.31}$$

where $\mathbf{D}^{ep}_{\text{dev}}$ is the deviatoric constitutive matrix and $\mathbf{B}$ is a standard deformation sub-matrix. The generic term of the discrete gradient matrix operator $\mathbf{G}^{AB}$ is given by:

$$\mathbf{G}^{AB} = \int_{\Omega_e} \left[\nabla N^A\right] N^B \, d\Omega \quad , \qquad \text{where } \left[\nabla N^A\right] = \left[N^A_{,x} \, N^A_{,y} \, N^A_{,z}\right]^T \tag{3.32}$$

while the laplacian term L^{AB} can be expressed as:

$$L^{AB} = \int_{\Omega_e} \left[\nabla N^A\right]^T \left[\nabla N^B\right] \, d\Omega \tag{3.33}$$

Finally, $\mathbf{M}^{AB}$ is the "mass" matrices associated to the displacement field:

$$\mathbf{M}^{AB} = \int_{\Omega_e} \mathbf{N}^A \mathbf{N}^B \, d\Omega \tag{3.34}$$

The expensive monolithic solution of system (3.29) can be avoided by using an iterative procedure, in which the pressure projection $\mathbf{\Pi}^{(n+1,i+1)}$ is solved independently and explicitly. To this end, from the third equation, it is possible to express $\mathbf{\Pi}^{(n+1,i+1)}$ in terms of $\mathbf{P}^{(n+1,i+1)}$ as:

$$\mathbf{\Pi}^{(n+1,i+1)} = \left(\mathbf{M}^{-1}_{\boldsymbol{\tau}}\right)^{(n+1,i)} \mathbf{G}_{\boldsymbol{\tau}} \, {}^{(n+1,i)}\mathbf{P}^{(n+1,i+1)} \cong \overline{\mathbf{M}}^{-1} \mathbf{G} \, \mathbf{P}^{(n+1,i+1)} \tag{3.35}$$

The computation of the projections $\mathbf{\Pi}$ can be transformed in a straight-forward operation by neglecting the difference in the τ_e coefficient in adjacent elements and considering an approximate lumped mass matrix $\overline{\mathbf{M}}$.

One further approximation can be introduced to make the solution of the mixed system of equations more efficient from the computational point of view. This consists in an staggered scheme, keeping the projected pressure gradient constant during the equilibrium iterations within each time increment, taking it equal to the corresponding value at the end of the previous time step, that is $\mathbf{\Pi}^{(n+1,i+1)} \cong \mathbf{\Pi}^{(n)}$. This strategy has proved effective without loss of precision nor robustness.

From the above, the implementation of the GLS method is straight-forward; it is enough to delete the third equation in (3.29), together with the corresponding third column of the global matrix, to yield:

$$\left[\begin{array}{cc} \mathbf{K}_{\text{dev}} & \mathbf{G} \\ \mathbf{G}^T & -\left(\dfrac{1}{K}\mathbf{M}+\mathbf{L}_{\boldsymbol{\tau}}\right) \end{array}\right]^{(n+1,i)} \left[\begin{array}{c} \delta\mathbf{U} \\ \delta\mathbf{P} \end{array}\right]^{(n+1,i+1)} = -\left[\begin{array}{c} \mathbf{R}_1 \\ \mathbf{R}_2 \end{array}\right]^{(n+1,i)} \tag{3.36}$$

where the effect of the stabilization matrix $\mathbf{L}_{\boldsymbol{\tau}}$ is evident. For the OSGS, the stabilization matrix can be formally expressed as $\widehat{\mathbf{L}}_{\boldsymbol{\tau}} = \mathbf{L}_{\boldsymbol{\tau}} - \mathbf{G}_{\boldsymbol{\tau}}^T \mathbf{M}_{\boldsymbol{\tau}}^{-1} \mathbf{G}_{\boldsymbol{\tau}}$.

4 Numerical examples

The formulation presented in the preceding sections is illustrated below in a number of benchmark problems. The proposed mixed formulation is applied using *2D plane-strain 3-noded linear triangular* meshes. The examples involve *compressible* elasticity and the isotropic O-J_2-VVV model with exponential *softening*.

Calculations are performed with an enhanced version of the finite element program COMET [49], developed by the authors at the International Center for Numerical Methods in Engineering (CIMNE). Pre and post-processing is done with GiD, also developed at CIMNE [50].

The Newton-Raphson method, combined with a line search procedure is used to solve the non-linear system of equations arising from the spatial and temporal discretization of the weak form of the stabilized problem. Convergence of a step is attained when the ratio between the iterative and the incremental norm of the computed displacements is lower than 0.01 (1 %).

Values $c = 1$ and $c' = 1$ are used for the evaluation of the stabilization parameter τ_e the viscous regularization, respectively. Note that this values amount to a minimal, but substantial, perturbation of the classical problem.

4.1 Benchmark cases

In this section, some benchmark tests subjected to homogeneous states of strain and stress are used to assess the performance and versatility of the proposed O-J_2-VVV model.

The domain used is a 0.1×0.1 m^2 square, discretized as 2 3-noded linear triangular elements. Plane strain conditions are assumed. The straining is applied by imposing the X-displacement at the right edge of the square, at a constant

rate of 10^{-3} m/s, both for loading and the successive unloadings and reloading. Movement in the Y-direction is unrestrained.

The following material properties are assumed: Young's modulus $E = 10$ MPa, Poisson's ratio $\nu = 0.3$ (recall that $G = E/2\,(1+\nu)$, $K = E/3\,(1-2\nu)$), uniaxial damage stress $\sigma_o = 10$ KPa and mode II fracture energy $G_{II} = 30$ J/m^2.

In all cases, equal time steps are performed to complete the analyses, $\Delta t = 0.02$ s.

4.1.1 Rate independent behaviour

First, rate independent behavior is tested. Viscous effects in the elastic, plastic and damage components of the model are deactivated.

Figure 4.1 shows XX-stress vs. XX-strain curve for tensile straining along the X-axis, for three different values of the overlay parameter: $\beta = 0.9$, $\beta = 0.0$ and $\beta = 1.0$. It can be observed that the envelopes of the three curves nearly overlap; this is because the three model dissipate the same fracture energy. However, the partial unloading/reloading branches display the different essence of the component models. The elasto-plastic model ($\beta = 0.0$) unloads and reloads elastically, exhibiting inelastic permanent strains; on the other hand, the elasto-damage model ($\beta = 1.0$) unloads and reloads secantly, that is, through the stress-strain origin, exhibiting loss of stiffness. As expected, the behaviour of the overlay model ($\beta = 0.9$) represents a mixture of the two other limit cases. Notice how the overlay model exhibits a certain amount of hysteresis, due to plastic yielding upon unloading, even though the value of β is relatively high.

Figure 4.2 shows XX-stress vs. XX-strain curve for cyclic tensile/compressive straining along the X-axis, for three different values of the overlay parameter: $\beta = 0.9$, $\beta = 0.0$ and $\beta = 1.0$. It can be observed that the envelopes of the three curves overlap exactly, because the three model dissipate the same fracture energy. However, the partial unloading/reloading branches display the different essence of the component models. In particular, note how the plastic model ($\beta = 0.0$) reaches the yield surface both in tension and compression, shrinking accordingly. As before, the behaviour of the overlay model ($\beta = 0.9$) represents a mixture of the two other limit cases.

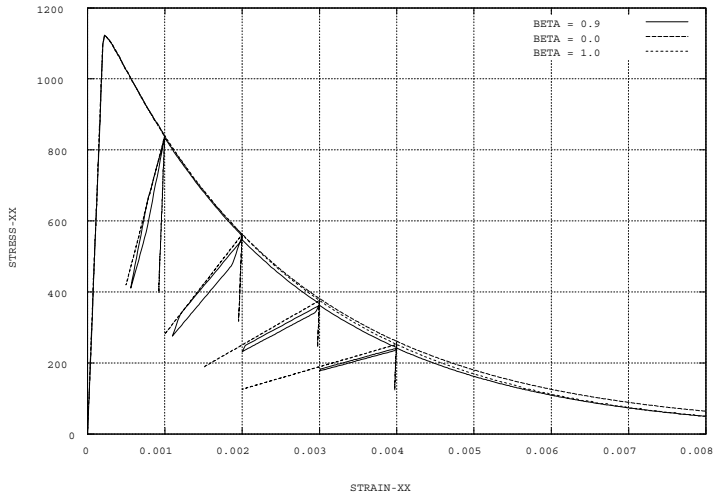

Fig. 4.1: Case 1. XX-stress vs. XX-strain for rate independent behaviour. Comparison for different values of β.

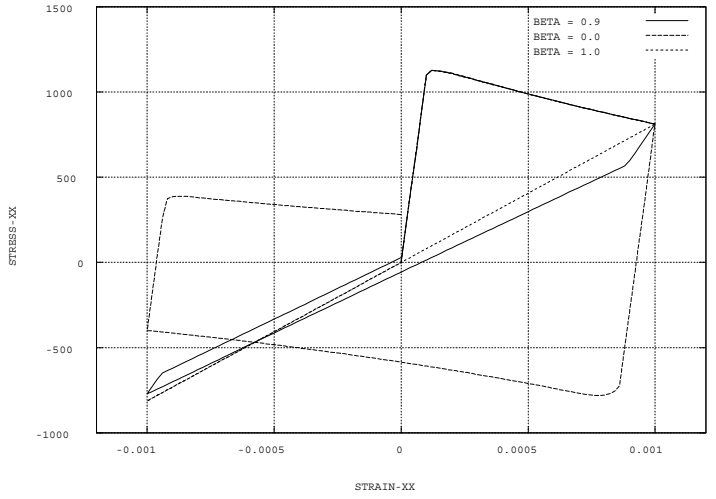

Fig. 4.2: Case 2. XX-stress vs. XX-strain for rate independent behaviour. Comparison for different values of β.

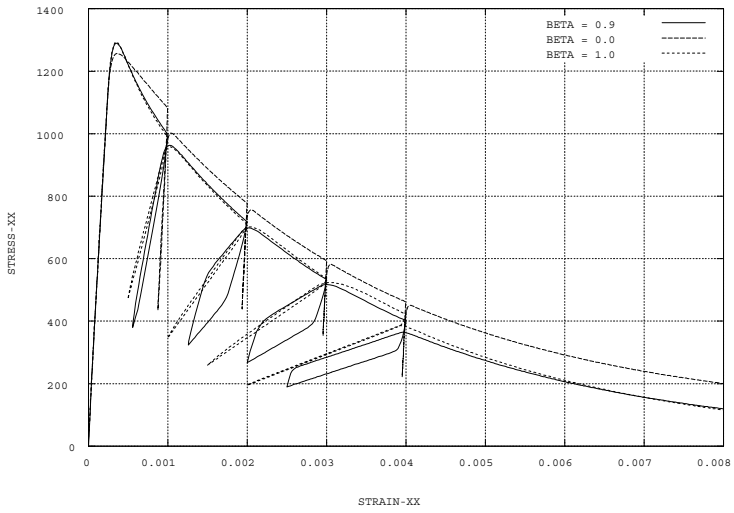

Fig. 4.3: Case 1. XX-stress vs. XX-strain for rate dependent behaviour. Comparison for different values of β.

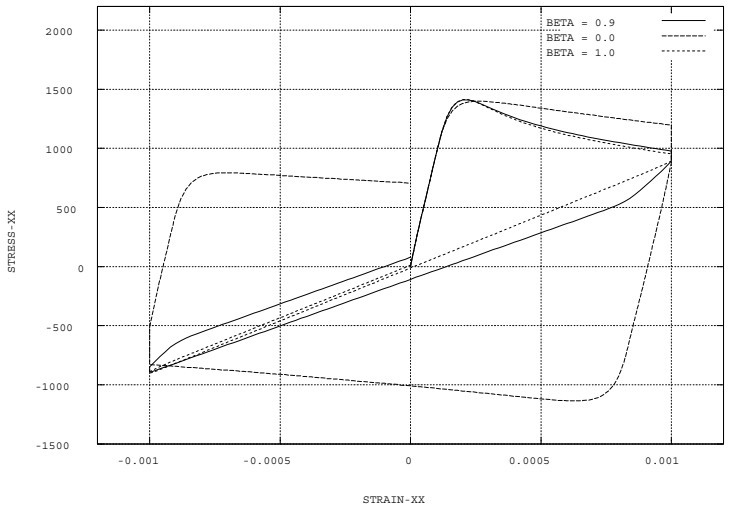

Fig. 4.4: Case 2. XX-stress vs. XX-strain for rate dependent behaviour. Comparison for different values of β.

4.1.2 Rate dependent behaviour

Now, rate dependent behavior is tested. To this end, viscous effects in the elastic, plastic and damage components of the model are activated. Viscoelasticity is modelled using two Maxwell elements ($N = 0, 1$) with the participation factors $\xi^0 = 0.75$, $\xi^1 = 0.25$ and the retardation times $\vartheta^0 = \infty$ and $\vartheta^1 = 0.05$ s. Viscoplasticity and viscodamage are controlled by identical retardation times $\vartheta^p = \vartheta^d = 0.05$ s.

Figure 4.3 shows XX-stress vs. XX-strain for tensile straining, three different values of the overlay parameter: $\beta = 0.9$, $\beta = 0.0$ and $\beta = 1.0$. The effect of the different viscous mechanisms is evident, comparing this Figure with Figure 4.1, where the rate independent cases where tested. Note how the peak stress is now higher due to the plastic and damage over-stresses. However, the initial stiffness is lower due to the viscoelastic component of the model. Notice also that viscoelasticity produces some hysteresis for all values of β. Even using the same retardation times, viscous effects affect differently the viscoplastic and viscodamage models. As before, the behaviour of the overlay model ($\beta = 0.9$) represents an average of the two other limit cases.

Figure 4.4 shows XX-stress vs. XX-strain curve for cyclic tensile/compressive straining along the X-axis, for three different values of the overlay parameter: $\beta = 0.9$, $\beta = 0.0$ and $\beta = 1.0$. Notice how viscosity affects differently the viscoplastic and viscodamage models. Note also that the even the viscodamage model ($\beta = 1.0$) exhibits a small amount of hysteresis, due to viscous effects.

4.2 Shear localization cases

In this section, two different examples are shown to assess the performance of the proposed O-J_2-VVV model in shear localization problems.

The following material properties are assumed: Young's modulus $E = 10$ MPa, Poisson's ratio $\nu = 0.3$, uniaxial damage stress $\sigma_o = 10$ KPa and mode II fracture energy $G_{II} = 200$ J/m^2. Rate dependent behaviour is considered. Viscoelasticity is modelled using two Maxwell elements ($N = 0, 1$) with participation factors $\xi^0 = 0.75$, $\xi^1 = 0.25$ and retardation times $\vartheta^0 = \infty$ and $\vartheta^1 = 0.05$ s. Viscoplasticity and viscodamage are controlled by identical retardation times $\vartheta^p = \vartheta^d = 0.05$ s.

It must be emphasized again that, in this examples, the dependent behaviour is not used to preserve the elliptic character of the problem, as similar, mesh objective, results can be obtained for the totally inviscid limits of the model, using the *OSGS* method, as shown in references [4] and [5].

In all cases 200 equal time steps are performed to complete the analyses, $\Delta t = 5 \times 10^{-4}$, so that $\Delta t/\vartheta^i = 100$.

4.2.1 Singly perforated strip

The first example is a plane-strain singly perforated strip subjected to axial imposed straining. Because of the double symmetry of the domain and boundary conditions, only one quarter of the domain (the top right quarter) needs to be discretized. Figure 4.5a depicts the original geometry of the problem; dimensions are 20×40 m^2 (width $\times$ height) and the radius of the perforation is $r = 1$ m. Thickness is 1 m.

The computational domain is divided into an unstructured uniform mesh of 7,336 linear triangles (3,801 nodes) with an average mesh size of $h_e = 0.25$ m, not shown. The pre-processor used tends to introduce patches or equilateral triangles with predominant directions at -30^o, $+30^o$ and $+90^o$ with the horizontal axis.

Figure 4.6 shows (half)-load vs (half)-imposed vertical displacement curves (recall 1 m thickness is assumed) obtained with three different overlay parameters:

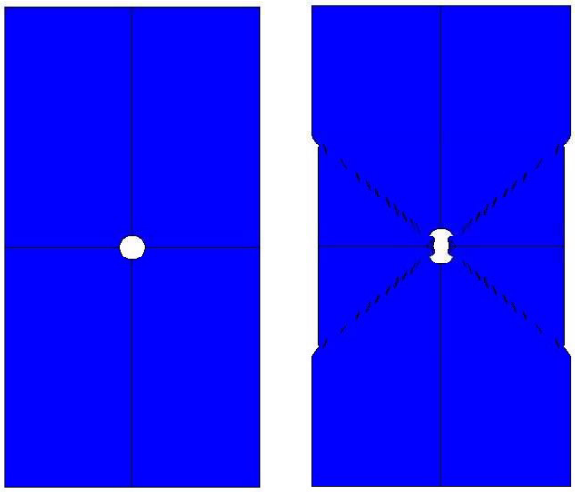

Fig. 4.5: Original and deformed (x 5) geometries for singly perforated strip

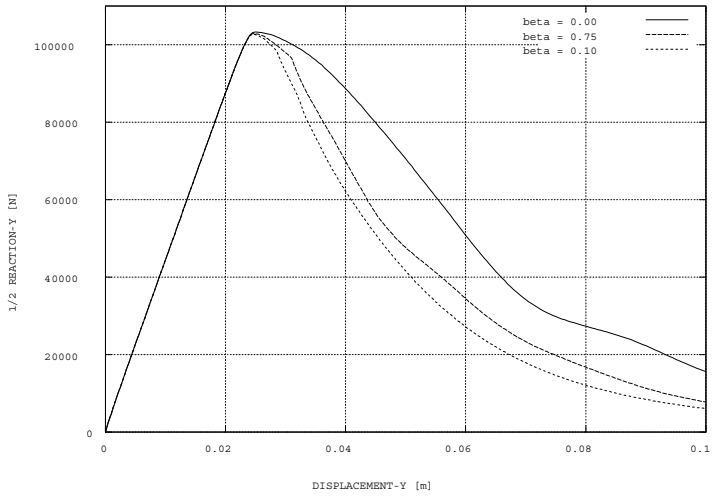

Fig. 4.6: Load versus displacement for simply perforated strip. Comparison among different β overlay parameter

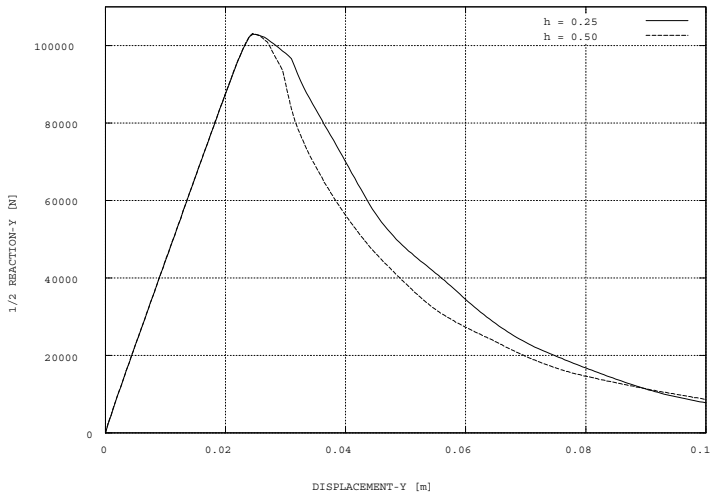

Fig. 4.7: Load versus displacement for simply perforated strip. Comparison between different mesh sizes. Overlay parameter $\beta = 0.75$

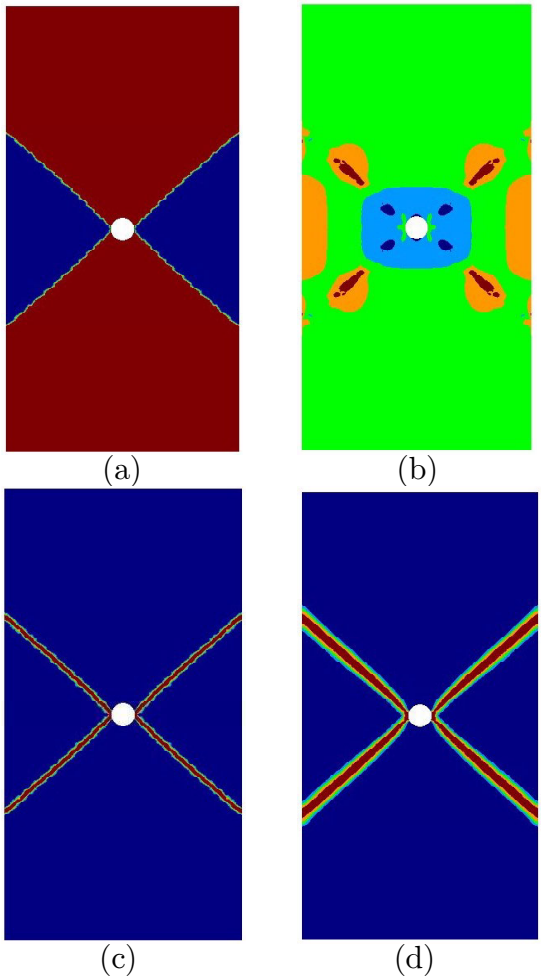

Fig. 4.8: Results for singly perforated strip. Contours for: (a) vertical displacement, (b) pressure (c) equivalent plastic deviatoric strain and (d) damage index

(a) $\beta = 0.0$, (b) $\beta = 0.75$ and (c) $\beta = 1.0$. Two remarks are in order. First, the three curves show a similar limit load, but the different essence of the component dissipative mechanisms show in the post-peak softening part curve. As it has been explained, the differences in the responses are due to the different unloading paths followed by the elements located outside the continuously narrowing shear localization band.

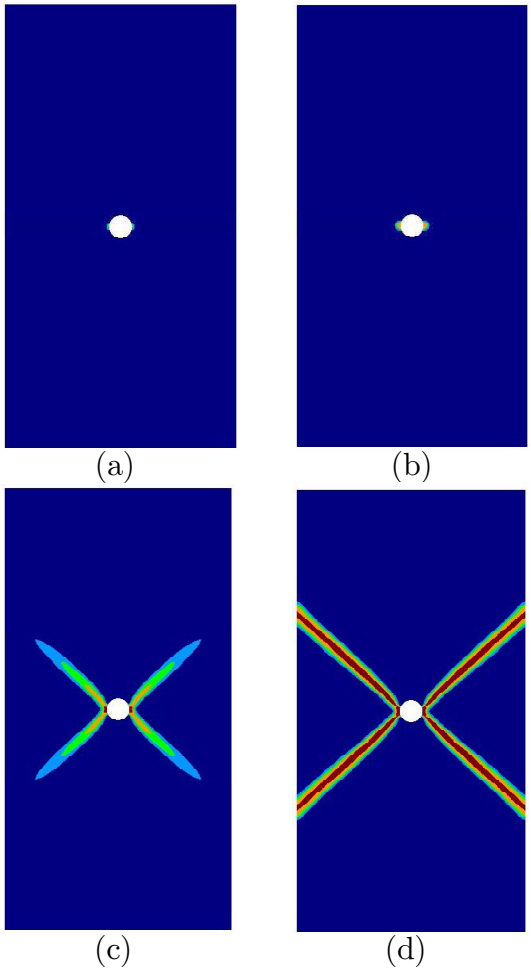

Fig. 4.9: Evolution of damage for singly perforated strip. Contours for (half)-imposed vertical displacement equal to: (a) 0.015, (b) 0.020, (c) 0.025 and (d) 0.030

Figure 4.7 shows (half)-load vs (half)-imposed vertical displacement curves (1m thickness is assumed) obtained with two uniform unstructured meshes with two element sizes: (a) $h_e = 0.25$ m and (b) $h_e = 0.50$ m (1,820 elements, 977 nodes). An overlay parameter $\beta = 0.75$ is used in this comparison. Note that the overall global response is satisfactorily similar upon mesh refinement, with the total area under the load-displacement curve converging to the correct amount of mechanical dissipation dissipated to create the localization bands. No spurious

brittleness is observed when the size of the elements is reduced. This is achieved by the regularization procedure of the plastic and damage softening moduli.

Figure 4.8 shows the results obtained using the proposed stabilized mixed $\mathbf{u}/p$ formulation, for a (half)-imposed vertical displacement $\delta = 0.10$ m, when the failure mechanism is already fully developed. Control on the pressure is completely attained, and no spurious oscillations are observed anywhere in the domain, even though a minimal amount of stabilization has been necessary (recall that $c = 1$ is used for the evaluation of the stabilization parameter τ_e). The resolution of the shear bands is optimal for the mesh used, as shown by the vertical displacement and equivalent plastic deviatoric strain plots. Discontinuity of the displacement tangential to the slip line occurs across one single element. The shear bands form a correct angle of approximately $\pm 45^o$ with the horizontal axis, irrespectively of the pronounced directional bias of the mesh. No indication of "overshoots"or "undershoots" of any magnitude is observed at either side of the discontinuity lines. The deformed shape of the strip (with an amplification factor of 5) is shown in Figure 4.5.

Finally, Figure 4.9 shows the evolution of the damage index at four different stages of the analysis, for: (a) $\delta = 0.015$ m, (b) $\delta = 0.020$ m, (c) $\delta = 0.025$ m and (d) $\delta = 0.030$ m. Note that the localization bands form completely at a very early stage of the analysis, and in a quite "explosive" fashion. The damage index of the elements inside the localization bands reaches values very close to unity, complete shear degradation, very early during the analysis.

4.2.2 Multiply perforated strip

The last example is a plane-strain strip with four circular perforations subjected to axial imposed straining. Because of the double symmetry of the domain and boundary conditions, only one quarter of the domain (the top right quarter) is discretized. Figure 4.10a depicts the original geometry of the problem; as in the previous examples, dimensions are 20×40 m^2 (width $\times$ height) and the radius of the perforations is $r = 1$ m. Thickness is 1 m.

The interest of this last example is that in it, as it will be shown below, the symmetric collapse mechanism consists of multiple shear bands that intersect each other and connect the perforations among them. Therefore, it is an adequate test to assess the ability of the different formulations to deal with such a complex situation.

The computational domain is divided into an unstructured uniform mesh of 7,353 linear triangles (3,823 nodes) with an average mesh size of $h_e = 0.25$ m.

Figure 4.11 shows (half)-load vs (half)-imposed vertical displacement curves (recall 1 m thickness is assumed) obtained with obtained with three different overlay parameters: (a) $\beta = 0.0$, (b) $\beta = 0.5$ and (c) $\beta = 1.0$. The remarks referred to the previous example also apply here.

Figure 4.12 shows (half)-load vs (half)-imposed vertical displacement curves (1m thickness is assumed) obtained with two uniform unstructured meshes with two element sizes: (a) $h_e = 0.25$ m and (b) $h_e = 0.50$ m (1,810 elements, 978 nodes). An overlay parameter $\beta = 0.75$ is used in this comparison. Once again, no spurious brittleness is observed when the size of the elements is reduced.

Figure 4.13 shows the results obtained using the proposed stabilized mixed $\mathbf{u}/p$ formulation, also for a (half)-imposed vertical displacement $\delta = 0.20$ m. The results obtained with this method are optimal, and only small spurious oscillations are observed in the pressure contours. These can be completely removed by slightly increasing the value of c used for the evaluation of the stabilization term. The resolution of the shear bands is optimal, as shown by the displacement and equivalent deviatoric strain plots, with the discontinuities occurring across one single element. The deformed shape of the strip (with an amplification factor of 5) is shown in Figure 4.10b.

Finally, Figure 4.14 shows the evolution of the damage index at four different

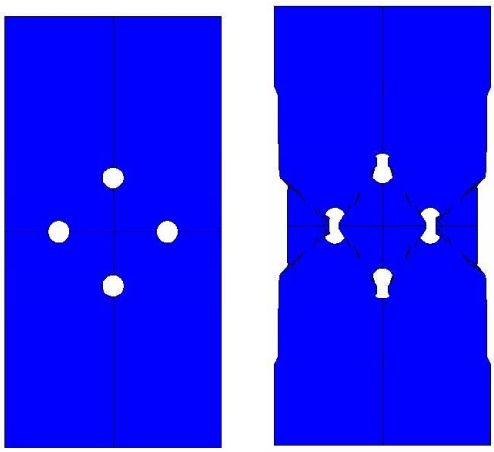

Fig. 4.10: Original and deformed (x 5) geometries for multiply perforated strip

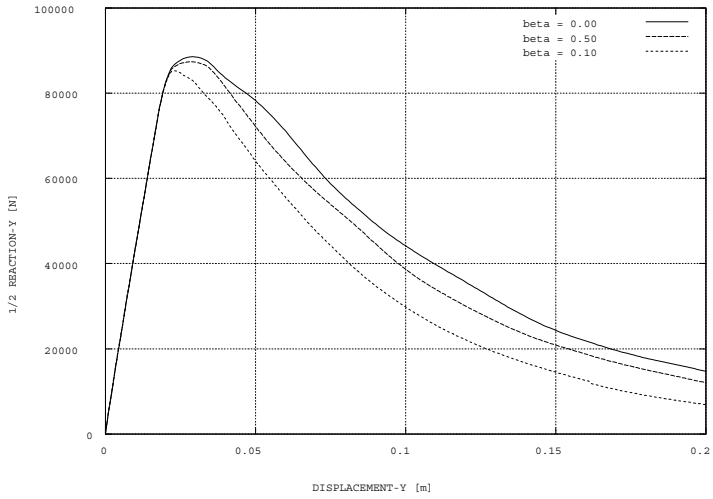

Fig. 4.11: Load versus displacement for multiply perforated strip. Comparison among different β overlay parameter

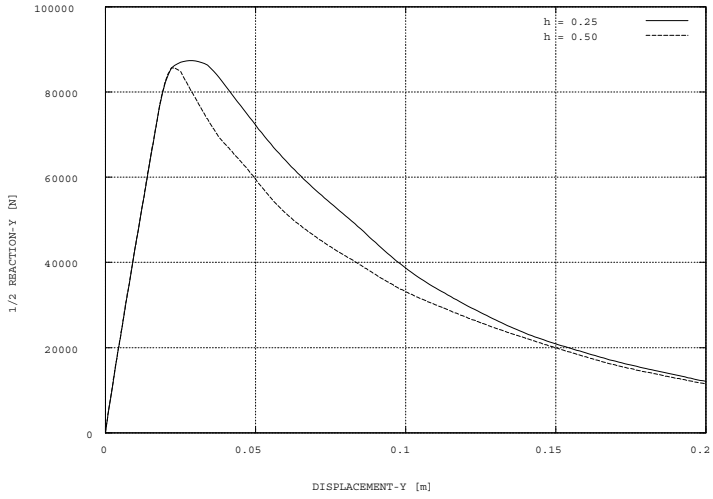

Fig. 4.12: Load versus displacement for multiply perforated strip. Comparison between different mesh sizes. Overlay parameter $\beta = 0.5$

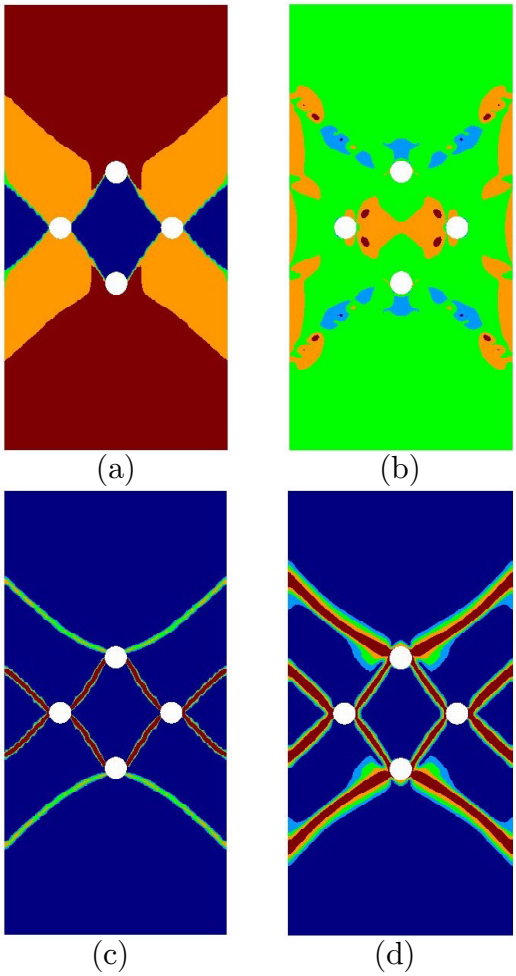

Fig. 4.13: Results for multiply perforated strip with OSGS formulation. Contours for: (a) vertical displacement, (b) pressure, (c) equivalent deviatoric plastic strain, (d) damage index

stages of the analysis, for a (half)-imposed vertical displacement: (a) $\delta = 0.020$ m, (b) $\delta = 0.030$ m, (c) $\delta = 0.040$ m and (d) $\delta = 0.060$ m. Notice how the central inner and outer shear bands develop first, while the upper and lower bands form at a later stage. Notice also that these later bands are not straight; regardless of this, the solution captures nicely such complicated failure mechanism.

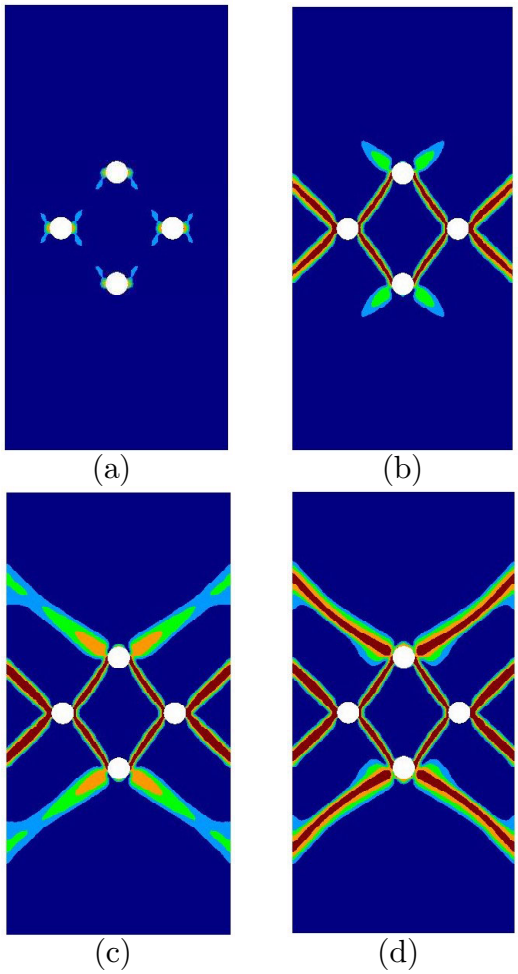

Fig. 4.14: Evolution of damage for multiply perforated strip. Contours for (half)-imposed vertical displacement equal to: (a) 0.020, (b) 0.030, (c) 0.040 and (d) 0.060

5 Conclusions

This work formulates an isotropic *overlay J2-Viscoelastic-Viscoplastic-Viscodamage model (O-J_2-VVV model)* that encompasses the merits of both the plastic and continuum damage formulations. This is a relatively simple constitutive model which, nevertheless, is able to reproduce realistic rate dependent (and, in the inviscid limit, rate independent) stress vs. strain responses which exhibit permanent strains and loss of stiffness upon unloading.

A fully stable formulation of the problem is obtained using the orthogonal sub-grid scales (*OSGS*) approach, which allows equal order interpolation of the displacement and pressure fields. This translates in the achievement of three crucial goals:

- (a) the solution of the corresponding localization boundary value problem exists and it is unique,
- (b) the position and orientation of the localization bands is independent of the directional bias of the finite element mesh, and
- (b) the global post-peak load-deflection curves are independent of the size of the elements in the localization band.

A consistent residual viscous regularization is proposed and successfully applied, in order to overcome the convergence difficulties often encountered in applications involving softening behaviour and shear strain localization.

The derived method yields a *robust* scheme, suitable for engineering applications in 2D and 3D.

Numerical examples show, first, the versatility of the model to reproduce rate dependent material responses; second, the tremendous advantage of the mixed

formulation over the irreductible one to predict correct failure mechanisms with localized patterns of shear deformation, completely free from any dependence of the mesh directional bias; and third, that stabilization techniques such as *OSGS* are able to fully avoid the volumetric locking exhibited by the standard non-stable formulations in the process of formation of shear bands, yielding a correct global response in the softening regime.

Acknowledgments

The authors gratefully acknowledge the invaluable help of our colleagues Prof. R. Codina and Prof. S. Oller, expressed in the form of unfailing suggestions and discussions.

Bibliography

[1] Chiumenti, M., Valverde, Q., Agelet de Saracibar, C. and Cervera, M., 2002. A stabilized formulation for incompressible elasticity using linear displacement and pressure interpolations, Comp. Meth. in Appl. Mech. and Eng., 191, 5253-5264.

[2] Chiumenti, M., Valverde, Q., Agelet de Saracibar, C. and Cervera, M., 2003. A stabilized formulation for incompressible plasticity using linear triangles and tetrahedra, Int. J. of Plasticity, to appear.

[3] Cervera, M., Chiumenti, M., Valverde, Q. and Agelet de Saracibar, C. 2003. Mixed Linear/linear Simplicial Elements for Incompressible Elasticity and Plasticity. Comp. Meth. in Appl. Mech. and Eng., in press.

[4] Cervera, M., Chiumenti and Agelet de Saracibar, C. 2003. Softening, localization and stabilization: capture of discontinuous solutions in J2 plasticity. Submitted to Int. J. for Num. and Anal. Meth. in Geomechanics.

[5] Cervera, M., Chiumenti and Agelet de Saracibar, C. 2003. Shear band localization via local J_2 continuum damage mechanics. Submitted to Comp. Meth. in Appl. Mech. and Eng.

[6] Cervera, M., Oliver, J., and Faria, R., 1995. Seismic evaluation of concrete dams via continuum damage models. Earth. Engng. Struc. Dyn., 24, 1225–1245.

[7] Cervera, M., Oliver, J., and Manzoli, O., 1996. A rate-dependent isotropic damage model for the seismic evaluation of concrete dams. Earth. Engng. Struc. Dyn., 25, 987–1010.

[8] Bazant, Z. P., editor (1988). Mathematical modelling of creep and shrinkage of concrete. John Wiley & Sons, New York.

[9] Carol, I. and Bazant, Z. P. (1993). Viscoelasticity with aging caused by solidification of nonaging constituent. J. Engrg. Mech., ASCE, 119, 2252–2269.

[10] Cervera, M., Oliver, J., and Galindo, M. (1992). Numerical analysis of dams with extensive cracking resulting from concrete hydration: simulation of a real case. Dam Engineering, 3, 1–22.

[11] Simo, J.C. and Hughes, T.J.R. 1998. Computacional Inelasticity. Interdisciplinary Applied Mathematics. Vol. 7. Springer.

[12] Bazant, Z.P. and Oh, B.H., 1983. Crack band theory for fracture of concrete. Material and Structures, 16, 155-177.

[13] Bazant, Z. and Pijaudier-Cabot, G., 1989. Measurement of characteristic length of non-local continuum. ASCE Journal of Engineering Mechanics, 115, 755-767.

[14] Jansen, D.C. and Shah, S.P., 1997. Effects of length on compressive strain softening of concrete. ASCE Journal of Engineering Mechanics, 123, 25-35.

[15] Oliver, J., 1989. A consistent characteristic length for smeared cracking models. Int. J. Num. Meth. Engng., 28, 461–474.

[16] Lemaitre, J. and Chaboche, J. L. 1978. Aspects phénoménologiques de la rupture par endommagement (in french). J. Méc. Appl., 2, 317–365.

[17] Simó, J. C. and Ju, J. W., 1987a. Strain- and stress-based continuum damage models - I. formulation. Int. J. Solids and Structures, 23, 821–840.

[18] Ju, J. W., 1989. On energy-based coupled elastoplastic damage theories: Constitutive modeling and computational aspects. Int. J. Solids and Structures, 7, 803–833.

[19] Luccioni, B., Oller, S. and Danesi, R., 1996. Coupled plastic-damaged model. Comp. Meth. in Appl. Mech. and Eng., 129, 81-89.

[20] Meschke, G., Lackner, R. and Mang, H.H., 1998. An anaisotropic elastoplastic-damage model for plain concrete. Int. J.. Num. Meths. in Engng., 42, 703-727.

[21] Menzel, A., Ekh, M., Steinmann, P. and Runesson, K., 2002. Anaisotropic damage coupled to plasticity: Modelling based on the effective configuration concept. Int. J.. Num. Meths. in Engng., 54, 1409-1430.

[22] Trusdell, C. and Toupin, R., 1960. The Classical Field Theories. Handbuch der Physik III/I. Springer, Berlin.

[23] Green, A. and Naghdi, A., 1965. A dynamical theory of interacting continua. J. Engng. Sci., 3-231.

[24] Ortiz, M. and Popov, E., 1982. A physical model for the inelasticity of concrete. Proc. Roy. Soc. London, A 383, 101-125

[25] Ortiz, M. and Popov, E., 1982b. Plain concrete as a composite material. Mech. Mater., 1, 139-150.

[26] Oller, S., Oñate, E., Miquel, J. and Botello, S., 1994. A plastic damage constitutive model for composite materials. Int. J. Solids and Struct., 33, 2501-2518.

[27] Car, E., Oller, S. and Oñate, E., 2000. An anisotropic elastoplastic constitutive model for large strain analysis of fiber reinforced composite materials. Comp. Meth. in Appl. Mech. and Eng., 185, 245-277.

[28] Aifantis, E.C., 1984. On the microstructural origin of certain inelastic models. Transactions ASME Journal of Engineering Materials Technology, 106, 326-330.

[29] Schereyer, H. and Chen, Z., 1986. One dimensional softening with localization. Journal of Applied Mechanics, ASME, 53, 791-797

[30] Vardoulakis, I. and Aifantis, E.C., 1991.A gradient flow theory of plasticity for granular materials.Acta Mechanica, 87, 197-217.

[31] de Borst, R. and Mulhaus, H.B., 1992. Gradient-dependent plasticity: formulation and algorithm aspect. Int. J.. Num. Meths. in Engng., 35, 521-539.

[32] Pamin, J., 1994. Gradient-Dependent Plasticity in Numerical Simulation of Localization Phenomena. Ph. D. Thesis, TU delft, The Netherlans.

[33] Peerlings, R.H.J., de Borst, R., Brekelmans, W.A. M. and Geers, M.G.D., 1998. Gradient-enhanced damage modelling of concrete failures. Mechanics of Cohesive-Frictional Materials, 4, 339-359.

[34] Jirásek, M., 1998. Nonlocal models for damage and fracture: comparison of approaches. Int. J. Solids and Structures, 35, 4133-4145.

[35] de Borst, R., 2001. Some recent issues in computational failure mechanics. Int. J. Num. Meths. in Eng., 52, 63-95.

[36] de Borst, R., 1991.Simulation of strain localization: a reppraisal of the Cosserat continuum. engineering computations, 8, 317-322.

[37] Steinmann, P. and Willam, K., 1992. Localization witin the framework of micropolar elastoplasticy. In Advances in Continuum Mechanics. ed. V. Mannl et al. pp. 296-313. Springer Verlag, Berlin.

[38] Brezzi, F. and Fortin, M., 1991. Mixed and Hybrid Finite Element Methods, Spinger, New York.

[39] Hughes, T.J.R. (1995). Multiscale phenomena: Green's function, Dirichlet-to Neumann formulation, subgrid scale models, bubbles and the origins of stabilized formulations, Comp. Meth. in Appl. Mech. and Eng.127, 387-401.

[40] Hughes, T.J.R., Feijoó, G.R., Mazzei. L., Quincy, J.B. (1998). The variational multiscale method-a paradigm for computational mechanics, Comp. Meth. in Appl. Mech. and Eng. 166, 3-28.

[41] Codina, R. (2002). Stabilized finite element approximation of transient incompressible flows using orthogonal subscales, Comp. Meth. in Appl. Mech. and Eng. 191, 4295-4321.

[42] Baiocchi, C., Brezzi, F. and Franca, L. (1993). Virtual bubbles and Galerkin/least-squares type methods (Ga.L.S.). Comp. Meth. in Appl. Mech. and Eng. 105, 125-141.

[43] Brezzi, F., Bristeau, M.O., Franca, L., Mallet, M. and Rogé, G. (1992). A relationship between stabilized finite element methods and the Galerkin method with bubble functions. Comp. Meth. in Appl. Mech. and Eng. 96, 117-129.

[44] Hughes, T.J.R., Franca, L.P. and Balestra, M. (1986). A finite element formulation for computational fluid dynamics: V. Circumventing the Babuska-Brezzi condition: A stable Petrov-Galerkin formulation of the Stokes problem accomodating equal-order interpolations. Comp. Meth. in Appl. Mech. and Eng. 59, 85-99.

[45] Hughes, T.J.R., Franca, L.P. and Hulbert, G.M. (1989). A new finite element formulation for computational fluid dynamics: VIII. The Galerkin/least-square method for advective-diffusive equations. Comp. Meth. in Appl. Mech. and Eng. 73, 173-189.

[46] Hughes, T.J.R., 1995. Multiscale phenomena: Green's function, Dirichlet-to Neumann formulation, subgrid scale models, bubbles and the origins of stabilized formulations, Comp. Meth. in Appl. Mech. and Eng., 127, 387-401.

[47] Codina, R., 2000. Stabilization of incompressibility and convection through orthogonal sub-scales in finite element methods, Comp. Meth. in Appl. Mech. and Eng., 190, 1579-1599.

[48] Needelman, A., 1987. Material rate dependence and mesh sensitivity in localization problems. Comp. Meth. in Appl. Mech. and Eng., 67, 68-75.

[49] Cervera, M., Agelet de Saracibar, C. and Chiumenti, M., 2002. COMET: COupled MEchanical and Thermal analysis. Data Input Manual, Version 5.0, Technical report IT-308, www.cimne.upc.es.

[50] GiD: the personal pre and post-processor, 2002. www.gid.cimne.upc.es.